Micro-Particle Operations Using Asymmetric Traps

by

Jae Sung Lee

A dissertation submitted in partial fulfillment
of the requirements for the degree of
Doctor of Philosophy
(Chemical Engineering)
in the University of Michigan
2017

Doctoral Committee:

Professor Mark A. Burns, Chair
Professor David T. Burke
Professor Ronald G. Larson
Professor Robert M. Ziff

Jae Sung Lee

netjigi@umich.edu

ORCID id: 0000-0003-4370-342X

To my family

Acknowledgment

It has been so long to come to this far. A few years ago, I thought one day that I might have graduated if a little bit more luck came to me. But, the truth is that it might have been longer or ended without the degree if I did not have great people around me. At the time that the next chapter of my life is about to begin, I would like to thank those who willingly gave their hand to me in the hardest time of my life. If your name is not here, it is not because your help was not meaningful, but because I unwittingly missed your name in a hurry for the submission of the dissertation. I sincerely apologize for my mistake and promise to become a better person.

At first, I would like to express my greatest gratitude to my family. My mother, Hyesook Lim, and father, Kwangsoo Lee, have always supported me regardless of the achievement I made. Whenever I need help, they were always there and became a strong support I can lean on throughout this prolonged doctoral course. Without their financial and mental support, I would not have been able to become a doctor. My sisters, Hyunjoo Lee and Sookyung Lee, also helped me become more professional. Especially, Sookyung, as a senior in academia, gave me much advice and became an exemplary of how to live as a scholar. My parents-in-law, Myungwan Kim and Sungsook Choi, also provided me with strong support to finish the dissertation work.

Next, I would like to express both my sincere apology and gratitude to my doctoral advisor, Prof. Mark A. Burns. He has had a hard time to manage a student who

was not truly ready to do Ph.D. course in a foreign country but who had a self-portrait little bigger than reality. I remember how I joined the Burns group. I think it would be an unexpected event for him, but he still gave me a chance to earn a Ph.D. degree, much advice to conduct research in his extremely busy schedule, and patiently waited for me to grow from a naïve child full of research dreams to an independent scholar who can willingly go through any hardship in doing research.

Also, I would like to thank Prof. David Burke, Prof. Ronald Larson, and Prof. Robert Ziff for being my committee. Although I have not had particularly many conversations or talk with them because I had a wrong idea in the early time of my Ph.D. course that Ph.D. students must be able to solve their project by themselves, even a few questions or advice they gave me during my study eventually helped me a lot. I still remember Prof. Burke's question in my preliminary exam. In the exam, he asked me when I would finish current project and start the next work. It would not be a hard question at all to most of the students. But, at that time, it was the question I have never thought about, and I did not have a good answer. At the time of publishing my first journal paper, I realized how important the question was and how ignorant about conducting research I was. Also, Prof. Larson has always been a great exemplary of academic scientist for his intelligence and limitless curiosity. Prof. Ziff has been very kind and humorous person who made the graduate years more enjoyable.

As I have stayed in Ann Arbor for a long time, I met many graduate students and staff in Burns group and Chemical Engineering Department. I think I have been so fortunate that all of Burns group members were great people as both colleagues and friends. Brian Johnson's touch is on every part of my experimental set-up. I greatly

appreciate for his contribution to the group. He was a great person and wonderful father of eight children. If he had not been there, I would not have been able to earn a Ph.D. Former Burns group members are people I owe a lot, too. Dustin Chang, Sean Langelier, Jihyang Park, Ramsey Zeitoun, Colin Jennings, Eric Livak-Hale were very smart and hilarious people who helped me get used to the new environment in the foreign country. Particularly, I cannot give enough thanks to Jihyang Park, who was both a lab mate in Ann Arbor and a classmate of my undergraduate school. She helped me everything of my Ann Arbor life from the beginning of my U.S. life to socialization in the grad school. I also would like to thank current Burns group members, Lavinia Yunzi Li, a recent graduate of Burns group, Stephen Sida Wang, Wen-Chi Lin, Liang Zhang, Zach Pritchard, Martin de Beer, Ioana Ciuta, Alyse Krausz, and Dr. Sarah Mena. Lavinia was a very kind and social person who helped a lot both by research and group life. I particularly enjoyed listening to her story about the journey for foods. My office mate, Wen-Chi Lin, was also a great person who had a great sense of responsibility and knew how to live a life. I enjoyed talking with her about diverse issues from cultural differences to politics of our home countries. I also would like to send special thank to hilarious guys, Liang Zhang, Zach Pritchard, and Martin de Beer, for making time in Burns group more enjoyable. I also thank Dr. Sarah Mena, the only postdoctoral scholar I've met in Burns group, for her showing a role model as a postdoctoral scholar. I am still learning a lot from her. I also remember my doctoral course classmates, Shi Yu and Segun Adegoke. We were international students who had cultural background quite different from the one in the United States. The conversation with them provided me with emotional support to endure hardships during long Ph.D. course. Among kind and

diligent staff in Chemical Engineering, I particularly would like to send my gratitude to Susan Hamlin and Kelly Raickovich. Susan, a graduate coordinator, always kindly answered to many questions I asked her and offered great help despite in many times I asked for her help at the last minute. Kelly Raickovich was a warm-hearted person who always took care of me and other Burns group members. I appreciate her for her great kindness and services.

Also, I must acknowledge Korean graduate students I have met in Ann Arbor, Dongil Kang, Yoonseob Kim, Taehyun Kim, Changyeop Seo, Sangmin Lee, Yein Lim, Sungjoo Kim, Gibeom Kwon, Jaeyoung Kwon, and Sun Ung Kim. Forgive me that I don't explain all of you in detail. But, I sincerely thank you for your support for me. The times to share the issues we had in our graduate work in our mother tongue were a great relief for me to continue and finish my work.

Lastly, there is one person who changed my whole life. My wife, Hyelim Seo, is the one who contributed the most to my growth as a person and a scholar. Since our relationship started, her deep thought from her unbelievable intelligence completely changed my view of the world and myself. Someone might say it is a lame expression, but the beginning of our marriage was a collision between two different worlds. During the time of identifying and understanding our differences, I learned how to communicate and share different ideas and feelings, which I believe was the most critical for not only finishing my Ph.D. course but also growing from an immature person to an adult person who genuinely knows what the responsibility is. I believe that she is the greatest gift in my life. I love you.

TABLE OF CONTENTS

LIST OF FIGURES

LIST OF APPENDICES

APPENDIX

ABSTRACT

Micro-particles are a great tool to detect biomolecules for their high multiplexing capability, wide options of materials, and scalability. Currently, most of the platforms utilizing micro-particles are bench-top scale instruments equipped with bulky devices for fine spatiotemporal control of micro-particles. This requirement for resources restricts the environment where micro-particles can be applied. To this problem, microfluidic techniques are an attractive solution because of its inherent capability of fine controlling of micro-particle due to scale matching.

This dissertation describes the development of the micro-particle operations using the asymmetric trap, a new mechanical trap that has flow direction dependent particle capturing behavior. Based on the theory of deterministic lateral displacement of micro-particle in periodic obstacle array and mass balance relationships, we provide a model that connects characteristic trap-particle interactions to critical dimensions including particle diameter and the gaps of the asymmetric traps. We theoretically predicted and experimentally observed five different trap-particle interactions including one-way particle transport, symmetric passage, symmetric capturing, trap skipping in zig-zag mode, and trap skipping in bump mode. Our model could explain most of the experimental results (particle diameter = 20.3 μm, $Re < 0.01$).

Based on our modeling of particle dynamics in the asymmetric traps, we explore micro-particle operations using the asymmetric traps. One-way particle transport, the

basic transport function using asymmetric traps, could displace hundreds of micro-particles across trap rows in only a few fluid oscillations (<500 ms per oscillation). On top of that, the segregation, medium exchange, and focusing and splitting of micro-particle in oscillatory flow were accomplished by capitalizing on two features: difference in the transport speeds of the trap-particle interaction dynamics and transport polarity of the asymmetric traps. At first, segregation of micro-particle mixture was achieved by utilizing the difference in transport speeds of trap-particle interaction dynamics. In the investigation of factors of the segregation performance, we found that the number of rows is the critical factor for a high performance of the segregation. Next, medium exchange of the particles in oscillatory flow was successfully demonstrated. At modest amplitude and number of fluid oscillations, the particle could be displaced into a new medium over the mixing region. Lastly, we could focus and split of groups of micro-particles in a few fluid oscillations by exploiting transport polarity of the asymmetric traps.

CHAPTER I

INTRODUCTION

1.1 Motivation

Over the last decade, micro-particle suspension, objects suspended in liquids whose diameters range from ~2 to ~100 μm, have been a workhorse that has greatly promoted the advance of life science and medical diagnostics. Flow cytometry utilizing microbeads enabled quantitation of molecular entities including proteins, nucleic acids, and metabolites at reduced time and cost while keeping sensitivity, reproducibility, and simplicity of conventional methods. [1] The superb multiplexing ability of the flow cytometry also allows system-level understanding of biological system of molecular networks and pathways of physiology and disease. [2] The micro-particle-based analysis is also available with cheaper detection platforms such as a simple plate reader or conventional optical microscope, which contributed to wide use of micro-particles. Lastly, micro-particles filled with magnetic entities are the most frequently used tool for automated isolation of cells or biomarkers. [3,4]

This popularity of micro-particles suspensions can be attributed to easy separation, multiplexing capability, wide options of available materials, and scalability. [5] The micro-particle suspended in fluid is basically two-phase system, which facilitates separation of molecules transferred from fluid to the surface of the micro-particle. Also, micro-particles have high multiplexing capability that has evolved with the advance of optics and micro-fabrication technologies. In current bench-top instruments, the number of detectable molecules from a single sample has already reached up to several hundreds. Optical encodings using oligo nucleotides [6] and nanoparticles [7] such as quantum dot [8] and photonic crystal [9] have been reported. The materials of micro-particles are almost limitless, ranging from polymeric materials such as polystyrene (PS) and polymethyl methacrylate (PMMA) to glass. These wide options of the materials enable the micro-particles to deal with countless number of diverse bio-chemicals. The size and number of micro-particles can be tuned easily to various assay conditions including concentration and sample volume.

To exploit those outstanding merits of the micro-particles, spatial control is the most basic, yet significant unit operation. The general procedure of chemical detection using micro-particles consists of unit operations from transport to mixing, and to separation. Although the purposes of those operations are different, they commonly require flexible displacement of micro-particles separately from surrounding medium. Since the suspension of micro-particles is always subject to the movement of the fluids, a discreet design of the control system is essential for spatial control of micro-particles independent of the movement of the fluids.

The techniques based on microfluidics can be a good option for fine control of micro-particles. Microfluidics is the field of study that utilizes characteristic physical properties of the fluids in small scale (~10-100 μm). In this scale, the effect of viscous force becomes dominant over inertial force, which means the fluid dynamics becomes deterministic and predictable. [10] Also, the scale matching between microfluidic channel and micro-particles provides fluidic forces such as shear force and lift force with fine resolution. This fine resolution enables individual control of a single micro-particle.

1.2 Microfluidic Techniques for Particle Operations

Current microfluidic techniques for particle operations can be categorized into active techniques and passive techniques. The active techniques incorporate the structure to apply external force field such as magnetic- and electric field. On the other hand, the passive techniques solely rely on fluidic forces and shape of streamlines. The choice of technique depends on available resources for implementation and nature of samples.

Magnetophoresis is the most popular active technique, which controls the particle that containing magnetic entity based on magnetic induction. The fluids where biological reactions occur are generally permeable to magnetic field and those reactions are independent of the magnetic field, so external magnetic field located outside of the devices can flexibly displace magnetic beads in fluidic chamber regardless of the fluid movement. [11] Therefore, magnetophoresis has been used for isolation of biomolecules from specimens in many commercialized portable point-of-care devices. [12,13] The

barrier for using magnetophoresis is the cost of magnetic beads and difficulty of fine control of groups of particles due to interference of magnetic fields.

Particle control using dielectrophoresis capitalizes on particle movement in non-uniform electric field. Depending on the electric dipole moment of a micro-particle and the frequency of alternating electric field, the particles move toward or away from the area of stronger electric field. [14] The dielectrophoresis is generally label-free and the dielectrophoretic force favors the small scale of the microfluidics due to the scaling of dielectric force with L as $F_{dep} \sim V^2/L^3$, where V the electric potential and L the characteristic length of the system. [15] The dielectrophoresis has been used for trapping and sorting of micro-particles [16,17] and many different cells such as platelets, [18] circulating tumor cells, [19] and bacteria. [20]

Next active technique is the optical tweezer. It uses intensity gradients of focused laser beam, and a particle is drawn to the focus of the beam. [21,22] It has very fine resolution, and on-demand generation and removal of electromagnetic field is achievable. The restraints of the technique are high cost and instrumental requirements for optical set-up. Also, the force of optical tweezer is generally not large enough to hold non-Brownian micro-particles in the presence of fluid flow. The optical tweezer is now fervently being used in the area called “Optofluidics” which combines fluidics and optics for the manipulation of micro- and nano-scale objects. [23] The optical tweezer has been utilized for particle sorting and multiplexed biochemical detection. [24,25]

Acoustic wave is also a good option for controlling micro-particles suspended in liquids. The acoustic wave has been used in two different forms: surface acoustic wave

(SAW) and acoustic streaming. [26,27] The surface acoustic wave is the acoustic wave propagating elastic surface, and acoustic streaming is a fluid flow generated by the damping of an ultrasonic wave. Drops and bubbles are popular sources that locally generate the acoustic streaming so that the particles are trapped in the circular fluid flow. [28] Both of the acoustic wave-based techniques have been applied to trapping and sorting of micro-particles, droplets, and cells. [29,30]

On the other hand, simple mechanical filtering is the most basic mean to control location of the micro-particles. It traps a micro-particle at a constriction whose separation is less than the diameter of the particle. There are three types of mechanical traps: weir, pillar, and pore. [31] For the best performance of mechanical trap, the concentration of micro-particles and capacity of the traps must be taken account of in the design phase. Otherwise, clogging due to arch formation can harm the yield and purity of the filtered product.

Deterministic lateral displacement is a representative technique that utilizes periodic pillar array. [32] The relative size of the particle to the gap between pillars and row shift fraction determine the transport mode including zig-zag mode and bump mode. [33] The lateral displacement of bump mode is greater than it of zig-zag mode, so the slanted pillar array can separate micro-particles by their size differences. Bump mode can guide the particles to any desired direction, which enabled complex path of the particles in the pillar arrays. [34] The particles processed by this technique ranges from entangled DNA of sub-micrometer scale to non-Brownian micro-beads.

Another important technique in the history of microfluidic passive techniques is inertial microfluidics. Inertial microfluidics exploit an inertial force of fluid at the flow regime of intermediate range of Reynolds number (~1 < Re < ~100). [35] In this intermediate flow, the inertial force of the fluid is not negligible, and a particle in a straight fluidic channel migrate to an equilibrium cross-sectional location that balances channel wall-induced lift force and shear gradient-induced lift force. This equilibrium position depends on the particle's physical properties such as diameter and density. The inertial microfluidics has an advantage of high-throughput due to relatively high flow rate compared to other microfluidic passive techniques. It has been utilized for many applications such as focusing, [36] separating, [37] and medium exchange [38] of micro-particles. The inertial microfluidics has recently extended its area to shape- and deformability- based separation of micro-particles. [39,40]

Besides the techniques described above, there have been other passive techniques that utilized the flow field shaped by the geometry of microfluidic channels or fluidic forces. The pinched flow fractionation separate micro-particles by amplifying the slight difference of the lateral positions in the pinched fluid segment through broadening of the fluid segments. [41,42] The hydrophoresis controls the cross-sectional position of micro-particles based on the movement of the particles in the pressure field created by slanted obstacles in fluidic channel. [43] Hydrodynamic microparticle railing transports micro-particles via railing on the square-shaped posts that arrayed at a small angle with respect to the fluid flow. [44] This technique is particularly advantageous for multi-step reaction.

1.3 Time-dependent Flow Field: Oscillatory Flow

Although passive techniques have evolved in many aspects such as size-resolution of the operations, throughput, a technique based on time-dependent varying fluid field has been unexplored. Most of current passive fluidic techniques rely on continuous flow. This dominant use of continuous flow partially comes from the use of a constant pneumatic pressure or the most abundant tool, a syringe pump, in the labs studying microfluidics. The microfluidic technique independent of those power sources can open a new chance for its use.

Oscillatory flow, a time-dependent flow field that has no fluid displacement at a period of fluid oscillation, has several advantages that can widen the area where passive techniques are applied. At first, the operations based on oscillatory flow can be implemented in a closed fluidic circuit, ex. a fluidic channel isolated by valves, so oscillatory flow-based technique can be easily integrated in the microfluidic devices for cell processing that needs to minimize human intervention between processes. Also, the use of oscillatory flow can further reduce the footprint of the device because no need of introductory region that is inevitable for achieving the proper conditions for passive techniques. The oscillatory flow can be easily coupled with simple alternate mechanical motion. This can be advantage for mobile devices having limited form factors.

1.4 Organization of this Dissertation

This dissertation will mainly discuss the development of oscillatory flow-based microfluidic technique for micro-particle operations. It starts from the development of the asymmetric trap, a mechanical trap having flow direction-dependent trap-particle interaction. Then, critical dimensions for elementary physical interactions including mechanical capturing and asymmetry are quantified by finding boundary streamline on which the particle starts those interactions. The modeling of trap/particle interactions is further extended to include multiple rows of the asymmetric traps. To predict particle dynamics in reverse flow, the theory about lateral displacement of micro-particle in periodic obstacle array is added to the model. Finally, the correlation between physical dimension of the system and the regimes of the trap/particle interaction is found. The microfluidic device for experimental validation is fabricated and proves the validity of the modeling. The knowledge about relation of trap/particle interaction to dimension of the system is used to devise the operations of micro-particle using asymmetric traps. The operations using asymmetric traps include segregation, medium exchange, and focusing and splitting of micro-particles.

Chapter 2 introduces the basic concept of the asymmetric trap, a mechanical trap having flow direction-dependent trap-particle physical interaction. The central method to find critical particle diameters for a trap-particle interaction is explained. It is based on the assumption that the particle moves in the direction to which more than half of the particle diameter belongs. The mass balance equation and flow field obtained at the absence of the particle in quasi-two dimensional system are used. The separate

experiments for both forward and backward flow validate the theoretical thresholds for mechanical capturing and asymmetry behavior.

In chapter 3, the particle dynamics in multiple rows of the traps in oscillatory flow is investigated. At first, the conditions for achieving positive net displacement of particle in oscillatory flow are defined based on the theory of fluid mechanics. Then, the prediction of the critical particle diameters for each condition is made by the theory about lateral displacement of microbead in periodic obstacle array and mass balance equations. For experimental validation of the modeling results, the set-up for oscillatory flow experiment is constructed. The device makes oscillatory flow across the asymmetric traps by cyclically actuating flexible polydimethylsiloxane (PDMS) membranes connected to each end of the asymmetric traps. Observed particle dynamics at about 50 different dimensions confirms the presence of five regimes of trap/particle interactions and its relationship with particle diameter and the gaps of the asymmetric traps.

Chapter 4 explores micro-particle operations achievable with the asymmetric traps. Combining the knowledge about five different types of the trap-particle interactions and transport polarity of the asymmetric traps, several functions are demonstrated. Particle segregation is conducted by using the difference in the transport speed of two different trap-particle interaction dynamics. In this dissertation, the particle in the regime of one-way particle transport is segregated from the particle in the regime of symmetric capturing. The effect of the capacity of the asymmetric trap array, particle concentration, and the amplitude and number of oscillation are also investigated. Medium exchange is presented by displacing the micro-particles initially suspended in one medium to the

other fluid. Finally, particle focusing and splitting by two arrays of opposite directions are demonstrated.

Chapter 5 concludes the dissertation with a summary of the work and a guide to possible future directions. The work described in this dissertation has a potential to realize the benefits of utilizing micro-particle in portable microdevices for resource-limited environment. To achieve that goal, several additional work needs to be done. At first, the operations of cells should be tested. Next, manual operation of the oscillatory flow is necessary. At third, the processing capacity of the device should be increased. Resolving these issues will be able to make a great impact on current field of portable point-of-care microdevices and integrated Lab-on-a-Chip device for cell processing.

1.5 References

1. J. Pataki, M. Szabó, E. Lantos, L. Székvölgyi, M. Molnár, É. Hegedüs, Z. Bacsó, J. Kappelmayer, G. Lustyik, and G. Szabó, Biological microbeads for flow-cytometric immunoassays, enzyme titrations, ad quantitative PCR, *Cytometry Part A*, 2005, **68**, 45-52.

2. J. P. Nolan and F. Mandy, Multiplexed and microparticle-based analyes: Quantitative tools for the large-scale analysis of biological systems, *Cytometry Part A*, 2006, **69**, 318-325.

3. J. J. Chalmers, M. Zborowski, L. Sun, and L. Moore, Flow through, immunomagnetic cell separation, *Biotechnology Progress*, 1998, **14**, 141-148.

4. Life Technologies, Surface-activated Dynabeads® A wide product portfolio for flexible molecular separations, brochure, 2010.

5. E. Verpoorte, Beads and chips: new recipes for analysis, *Lab on a Chip*, 2003, **3**, 60N-68N.

6. K. L. Gunderson, S. Kruglyak, M. S. Graige, F. Garcia, B. G. Kermani, C. Zhao, D. Che, T. Dickinson, E. Wickham, J. Bierle, D. Doucet, M. Milewski, R. Yang, C. Siegmund, J. Haas, L. Zhou, A. Oliphant, J.-B. Fan, S. Barnard, and M. S. Chee, Decoding randomly ordered DNA arrays, *Genome Research*, 2004, **14**, 870-877.

7. Y. Leng, K. Sun, X. Chen, and W. Li, Suspension arrays based on nanoparticle-encoded microspheres for high-throughput multiplexed detection, *Chemical Society Reviews*, 2015, **44**, 5552-5595.

8. M. Han, X. Gao, J. Z. Su, and S. Nie, Quantum-dot-tagged microbeads for multiplexed optical coding of biomolecules, *Nature Biotechnology*, 2001, **19**, 631-635.

9. Y. Zhao, X. Zhao, and Z. Gu, Photonic crystals in bioassays, *Advanced Functional Materials*, 2010, **20**, 2970-2988.

10. T. M. Squires and S. R. Quake, Microfluidics: fluid physics at the nanoliter scale, *Reviews of Modern Physics*, 2005, **77**, 977-1026.

11. M. A. M. Gijs, F. Lacharme, and U. Lehmann, Microfluidic applications of magnetic particles for biological analysis and catalysis, *Chemical Reviews*, 2010, **110**, 1518-1563.

12. C.-H. Wang, K.-Y. Lien, T.-Y. Wang, T.-Y. Chen, and G.-B. Lee, An integrated microfluidic loop-mediated-isothermal-amplification system for rapid sample pre-

treatment and detection of viruses, *Biosensors and Bioelectronics*, 2011, **26**, 2045-2052.

13. C.-H. Chiou, D. J. Shin, Y. Zhang, T.-H. Wang, Topography-assisted electromagnetic platform for blood-to-PCR in a droplet, *Biosensors and Bioelectronics*, 2013, **50**, 91-99.

14. B. Çetin and D. Li, Dielectrophoresis in microfluidics technology, *Electrophoresis*, 2011, **32**, 2410-2417.

15. J. Voldman, Electrical forces for microscale cell manipulation, *The Annual Review of Biomedical Engineering*, 2006, **8**, 425-454.

16. J. L. Baylon-Cardiel, N. M. Jesús-Pérez, A. V. Chávez-Santoscoy, B. H. Lapizco-Encinas, Controlled microparticle manipulation employing low frequency alternating electric fields in an array of insulators, *Lab on a Chip*, 2010, **10**, 3235-3242.

17. B. G. Hawkins, A. E. Smith, Y. A. Syed, and B. J. Kirby, Continuous-flow particle separation by 3D insulative dielectophoresis using coherently shaped, dc-biased, ac electric fields, *Analytical Chemistry*, 2007, **79**, 7291-7300.

18. N. Piacentini, G. Mernier, R. Tornay, and P. Renaud, Separation of platelets from other blood cells in continuous-flow by dielectrophoresis field-flow-fractionation, *Biomicrofluidics*, 2011, **5**, 034122.

19. P. R. C. Gascoyne and S. Shin, Isolation of circulating tumor cells by dielectrophoresis, *Cancers*, 2014, **6**, 545-579.

20. D. Cai, M. Xiao, P. Xu, Y.-C. Xu, and W. Du, An integrated microfluidic device utilizing dielectrophoresis ad multiplex array PCR for point-of-care detection of pathogens, Lab on a Chip, 2014, **14**, 3917-3924.

21. A. Ashkin, Optical trapping and manipulation of neutral particles using lasers, *Proceedings of the national academy of sciences of the United States of America*, 1997, **94**, 4853-4860.

22. D. G. Grier, A revolution in optical manipulation, *Nature*, 2003, **424**, 810-816.

23. D. Psaltis, S. R. Quake, and C. Yang, Developing optofluidic technology through the fusion of microfluidics and optics, *Nature*, 2006, **442**, 381-386.

24. M. P. MacDonald, G. C. Spalding, and K. Dholakia, Microfluidic sorting in an optical lattice, *Nature*, 2003, **426**, 421-424.

25. M. Manesse, A. F. Phillips, C. N. LaFratta, M. A. Palacios, R. B. Hayman, and D. R. Walt, Dynamic microbead arrays for biosensing applications, *Lab on a Chip*, 2013, **13**, 2153-2160.

26. X. Ding, P. Li, S.-C. S. Lin, Z. S. Stratton, N. Nama, F. Guo, D. Slotcavage, X. Mao, J. Shi, F. Constanzo, and T. J. Huang, Surface acoustic wave microfluidics, *Lab on a Chip*, 2013, **13**, 3626-3649.

27. M. Wiklund, R. Green, and M. Ohlin, Acoustofluidics 14: Applications of acoustic streaming in microfluidic devices, *Lab on a Chip*, 2012, **12**, 2438-2451.

28. S. S. Sadhal, Acoustofluidics 16: acoustics streaming near liquid-gas interfaces: drops and bubbles, *Lab on a Chip*, 2012, **12**, 2771-2781.

29. C. Wang, S. V. Jalikop, and S. Hilgenfeldt, Efficient manipulation of microparticles in bubble streaming flows, *Biomicrofluidics*, 2012, **6**, 012801.

30. C. Wang, S. V. Jalikop, and S. Hilgenfeldt, Size-sensitive sorting of microparticles through control of flow geometry, *Applied Physics Letters*, 2011, **99**, 034101.

31. C. Jin, S. M. McFaul, S. P. Duffy, X. Deng, P. Tavassoli, P. C. Black, and H. Ma, Technologies for label-free separation of circulating tumor cells: from historical foundations to recent developments, *Lab on a Chip*, 2014, **14**, 32-44.

32. L. R. Huang, E. C. Cox, R. H. Austin, and J. C. Sturm, Continuous particle separation through deterministic lateral displacement, *Science*, 2004, **304**, 987-990.

33. D. W. Inglis, J. A. Davis, R. H. Austin, and J. C. Sturm, Critical particle size for fractionation by deterministic lateral displacement, *Lab on a Chip*, 2006, **6**, 655-658.

34. K. J. Morton, K. Loutherback, D. W. Inglis, O. K. Tsui, J. C. Sturm, S. Y. Chou, and R. H. Austin, Hydrodynamic metamaterials: Microfabricated arrays to steer, refract, and focus streams of biomaterials, *Proceedings of National Academy of Sciences of the United States of America*, 2008, **105**, 7434-7438.

35. H. Amini, W. Lee, and D. Di Carlo, Inertial microfluidic physics, *Lab on a Chip*, 2014, **14**, 2739-2761.

36. S. C. Hur, H. T. K. Tse, and D. Di Carlo, Sheathless inertial cell ordering for extreme throughput flow cytometry, *Lab on a Chip*, 2010, **10**, 274-280.

37. A. J. Mach and D. Di Carlo, Continuous scalable blood filtration device using inertial microfluidics, *Biotechnology and Bioengineering*, 2010, **107**, 302-311.

38. D. R. Gossett, H. T. K. Tse, J. S. Dudani, K. Goda, T. A. Woods, S. W. Graves, and D. Di Carlo, Inertial manipulation and transfer of microparticles across laminar fluid streams, *Small*, 2012, **8**, 2757-2764.

39. S. C. Hur, S.-E. Choi, S. Kwon, and D. Di Carlo, Inertial focusing of non-spherical microparticles, *Applied Physics Letters*, 2011, **99**, 044101.

40. S. C. Hur, N. K. Henderson-MacLennan, E. R. B. McCabe, and D. Di Carlo, Deformability-based cell classification and enrichment using inertial microfluidics, *Lab on a Chip*, 2011, **11**, 912-920.

41. M. Yamada, M. Nakashima, and M. Seki, Pinched flow fractionation: Continuous size separation of particles utilizing a laminar flow profile in a pinched microchannel, *Analytical Chemistry*, 2004, **76**, 5465-5471.

42. J. Takagi, M. Yamada, M. Yasuda, and M. Seki, Continuous particle separation in a microchannel having asymmetrically arranged multiple branches, *Lab on a Chip*, 2005, **5**, 778-784.

43. S. Choi and J.-K. Park, Continuous hydrophoretic separation and sizing of microparticles using slanted obstacles in a microchannel, *Lab on a Chip*, 2007, **7**, 890-897.

44. R. D. Sochol, S. Li, L. P. Lee, and L. Lin, Continuous flow multi-stage microfluidic reactors via hydrodynamics microparticle railing, *Lab on a Chip*, 2012, **12**, 4168-4177.

CHAPTER II

THE INTERACTION OF ASYMMETRIC TRAP WITH MICRO-PARTICLES

2.1 Introduction

The method of selective particle transport, a technique necessary for many microfluidic applications, can be achieved using both active and passive particle manipulation techniques. Active techniques use non-fluidic forces to utilize inherent field-responsive properties of particles or of attached labels. Electrokinetic phenomena such as electrophoresis and dielectrophoresis use electric fields and intrinsic electric permittivity differences to achieve motion, [1,2] and magnetophoresis uses the magnetic susceptibility. [3] Light and sound can also be used as in optical tweezer, [4,5] and acoustic streaming, [6-9] respectively. These active techniques all need to generate the appropriate field in the device or to place the device under an external field generated by auxiliary instruments.

Current passive fluidic techniques use various working principles including mechanical trapping, streamline manipulation, and fluid inertia with mechanical trapping being the most common. [10-15] Deterministic lateral displacement can concentrate or separate particles based on the size of particles flowing through periodic obstacle arrays designed to divide a flow stream in certain fractions. [16-18] The variation of physical

dimension of the periodic array enabled a wide range of separable particle sizes from nm to μm. Inertial microfluidics can separate particles by size and density based on inertial lift force and Dean flow in confined channel geometries at intermediate Reynolds number regime (~1<Re<100). [19-21] Hydrodynamic filtration eludes [22] or spatially separates [23,24] particles at different lateral positions subject to parabolic flow profile in which the size of the particle limits accessible region of the profile. Sequence of cylindrical posts can be used to shape the cross-sectional profile of the fluid flowing through the posts, which, in turn, can cause particle separation. [25] The microvortex generated by slanted obstacles has been used to separate the particles of different sizes and densities. [26-28]

Recently, several passive fluidic techniques have afforded functions other than just capturing or separation. Iwai *et al.*, used the steric interaction between particles and pillar arrays to avoid capturing during reverse flow, retrieving the particles captured in the array. [29] Also, Sochol *et al.,* showed the flow polarity-dependent particle capturing array capable of the retrieval by introducing the fluidic channels having smaller width at the back of the trapping channels. [30] The fluidic channel which size is comparable to the particle could generate the amount of fluidic force enough to prevent the particle immobilization at the back of the trapping channels during reverse flow. In another work of the same group, the guided transport of microparticles and cells on a rail of microposts having low incident angle with respect to the flow was suggested. [31] The micropost rail could transport the microparticles through multiple layers of reagents for sequential multi-stage biochemical reactions. In subsequent work, the same group could insert traps

in the middle of the rail by adjusting the incident angle and the shape of the microposts, confirming the reaction progress with the signal from trapped microparticles. [32]

In this chapter, we demonstrate the use of an asymmetric trap array for size-selective particle transport. The physical dimensions for the array were theoretically formulated based on mass conservation equations for a quasi-two-dimensional system. Numerical simulations predicted five different regimes of the trap/particle steric interaction: symmetric passage (I), asymmetric passage (IIa), symmetric capturing (IIb), asymmetric capturing (III), and channel clogging (IV). Particle flow experiments at low Reynolds number regime ($Re < 0.01$) validated the regimes of trap/particle interaction.

2.2 Material and Methods

2.2.1 Fabrication of the microfluidic device

The PDMS (Polydimethylsiloxane) device was fabricated via PDMS double casting process. The photolithography and deep reactive ion etching made the first silicone master. The 5 um of thickness of photoresist (spr 220 3.0) was spincoated on Si wafer and baked at 150^{o}C for 90 sec (ACS200, Karl Suss MicroTec). The wafer was exposed of 360 mJ/cm^2 in the aligner (MA/BA-6 Suss) and was in rest at room temperature for 40 min. Then, the rested wafer was baked at 150^{o}C for 90 sec again and was developed by 30 sec washing in MIF300 developer in the ACS200. For the PDMS casting, the fabricated Si master was silanized with trichlorosilane ((Tridecafluoro-1,1,2,2-Tetrahydrooctyl)-1-Trichlorosilane, UCT) in a dessicator for 4 hours after the plasma treatment in reactive ion etcher (model and company name). Mixed PDMS (10:1

monomer:crosslinker mass ratio) was casted on the Si mold, degassed in 25 mmHg vacuum, and heated at 85^{o}C overnight. Fabricated PDMS mold was peeled from the Si mold, and silanized through the same processes done for the Si master. Then, finally mixed PDMS (10:1 monomer:crosslinker mass ratio) was poured on the PDMS master, degassed in 25 mmHg vacuum, and heated at 85^{o}C 4 hours in an oven. After the crosslinking, the casted PDMS was slowly cooled down to minimize the cracking caused by thermal stress. Crosslinked PDMS was carefully detached from the PDMS mold. Inlet and outlet of the device were made with 2 mm punch (Uni-Core, Harris). The PDMS block was cut and bonded to microslide through plasma activation of the surface by a plasma wand. The height of the channel was 27 μm for the particle of 20.3 μm diameter, and 17 μm for the particle of 10.1 μm diameter.

2.2.2 Numerical simulation

To obtain the flow profile at the gaps between trap elements, ComSol® 4.3 simulation package was used. The geometries of the array was drawn in L-Edit (v.12.11) and imported to the ComSol®. The row shift ratio of all the geometries was 1/3 and the size of barrier and trapping blocks were retained throughout the simulation. The array had 9 rows of 45 asymmetric traps, and flow profile in the fifth row was used. The boundary condition of wall of trap elements was no-slip condition, and the wall of the channel was set as periodic boundary condition to minimize the effect of the channel wall. The inlet condition was superficial flow 100 μm/s, and outlet condition was no pressure. In the mesh condition of extremely fine, maximum element growth rate and the resolution of narrow regions are modified as 1.1 and 15 to assure the quality of the simulation. The HP Z220 of Intel Ivy Bridge Quad 3.5GHz and 16GB RAM was used for the computing.

2.2.3 Flow Experiment

The raw particle solution (SPHERO^{TM} Fluorescent Nile Red 20.3 μm, Spherotech, and G1000 10.1 μm, Duke scientific corp.) was diluted 10X in the water solution mixed with Optiprep® density gradient medium (Sigma-Aldrich) and Tween20 (Sigma-Aldrich) surfactant (v/v 0.5 %) to equate its density to the density of the particle. For every flow experiment, the sample was freshly made and subject to the sonication for 5 min before the use. The sample was introduced through the pipet tip plugged into the inlet of the device. The flow through the device was made by hydrostatic pressure difference between the inlet and the outlet of the device.

The interaction regime of the array was confirmed by running two subsequent flow experiments of both flow directions in a single device which contained an asymmetric trap array of single trap/particle interaction regime. At first, the asymmetry was visually checked during upward flow. If no particles went through the trapping gap (s) during upward flow, the trap array was judged as asymmetric. Next, the capturing ability of the array was tested during backward flow. However, especially for the symmetric capturing regime, the capturing was also observed during upward flow as expected. The two different sizes (20.3 μm and 10.1 μm) of polystyrene beads were used. To avoid uneven flow rates at the two trapping gaps of an asymmetric trap, vertical spacing between the rows of asymmetric traps was retained at the twice the trap vertical size. The average velocity of the particle was generally on the order of 100 μm/s, and the Reynolds number was less than 0.1.

2.2.4 Imaging of trap/particle interaction

The trap/particle interaction was observed and imaged via Nikon Eclipse Ti microscope and QImaging Exi BLUE camera. The movies of the trap/particle interaction were recorded by the same camera at the frequency of 6.9312 fps.

2.3 Results and Discussion

2.3.1 Asymmetric trap

An asymmetric trap is composed of three separate obstacles: a pentagon-shaped barrier and two diamond-shaped trapping blocks (Figure 2.1.a). The pentagonal barrier prevents direct passage of a particle through the gap in the middle of the trapping blocks of the trap (Figure 2.1.b), and the shape of the pentagon minimizes possible particle trapping at the stagnation point of the barrier. The two trapping blocks are located at a set distance, s, from the top of the barrier. We call this vertical gap between the barrier and the trapping blocks the trapping gap. Particle with a diameter, d, greater than the trapping gap will become trapped in this region. Each asymmetric trap has two such mechanical trapping gaps.

The vertical asymmetry of the trap elements creates different outcomes depending on the flow direction with respect to the trap. During downward flow, a non-deformable particle larger than the trapping gap (i.e., d>s) is captured if the particle's streamline passes through the gap (Figure 2.1.b). On the other hand, during upward flow, the fluid passing through the gap releases the captured particle. A particle initially located below

the trap shifts streamlines through collision with the barrier and the particle and is not captured (Figure 2.1.c).

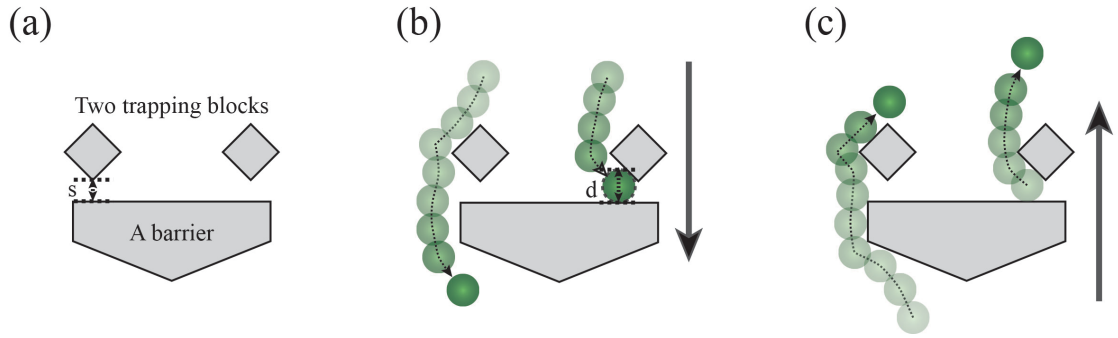

Figure 2.1: The asymmetric trap/particle interaction. (a) The structure of an asymmetric trap. (b) The particle-trap interaction during downward flow. (c) The particle-trap interaction during upward flow.

2.3.2 Asymmetry of trap/particle steric interaction

In an array of asymmetric traps, the horizontal location of the particle in the inter-barriers gap, g, after the trap/particle steric interaction determines the asymmetry of that interaction. During upward flow, the particle can shift streamlines when the particle contacts the barrier during upward flow. For particles on the same initial streamline, the particle of greater size is shifted a greater distance. If the central axis of the particle is located out of the fluid stream, flowing into the trapping gap (i.e., $d>d_c$ in Figure 2.2.a), the particle passes the row of the traps without being captured. It should be noted that the motion of the particle is assumed as purely shear-induced movement. Therefore, particles greater than the critical size ($d>d_c$) pass by the trap during upward flow and can flow into the trapping gap during downward flow; this motion is defined as asymmetric behavior

(Figure 2.2.b). On the other hand, particles smaller than the critical size ($d<d_c$) can flow into the trapping gap during flow in both directions; this motion is defined as symmetric behavior (Figure 2.2.c).

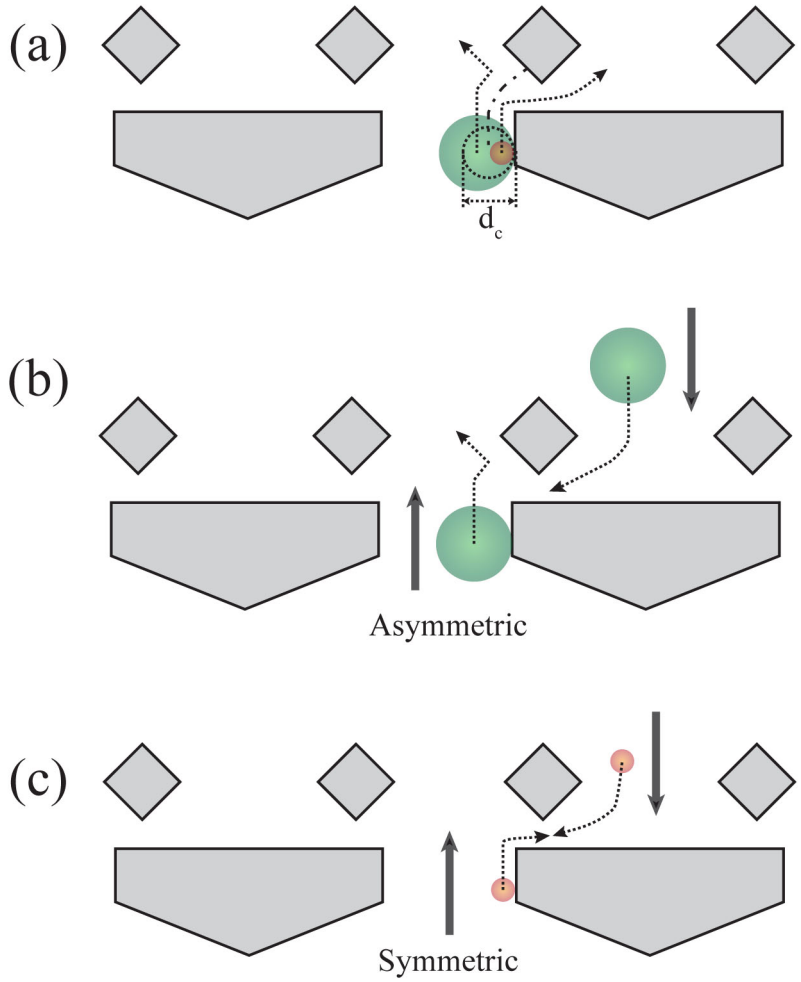

Figure 2.2: The effect of particle size on the asymmetric behavior of the trap. (a) Larger particles ($d>d_c$) cannot flow into the trapping gap during upward while smaller particles ($d<d_c$) can. (b) In asymmetric behavior, a particle travels on a different path in upward flow than in downward flow. (c) For symmetric behavior, the particle travels along the same path regardless of flow direction.

The width, w_s (Figure 2.3), of the trapping flow can be calculated based on the mass balance at the trifurcation point in the array. The flow, Q_g, entering the gap, g, is

divided into three separate flow streams: Q_s, Q_h, and an identical Q_s (Figure 2.3.a). Thus, Q_g is defined by a mass balance:

$$Q_g = 2Q_s + Q_h \tag{1}$$

We can define the width of the trapping flow, w_s, at g such that the flow rate through w_s equals Q_s,

$$\int_0^{w_s} v_g(x)dx = Q_s \tag{2}$$

Note that w_s is equal to a half of the d_c[21] shown in Figure 2.2 and determines the asymmetry of the trap/particle steric interaction. The assumption is that particles follow streamlines obtained in the absence of the particle, which means the perturbation of the particle surface on the streamline is negligible. It can be tentatively said that the error coming from this assumption has no effect in qualitative analysis and is negligible at the tested range of particle concentration (0.1~1% solid volume fraction).

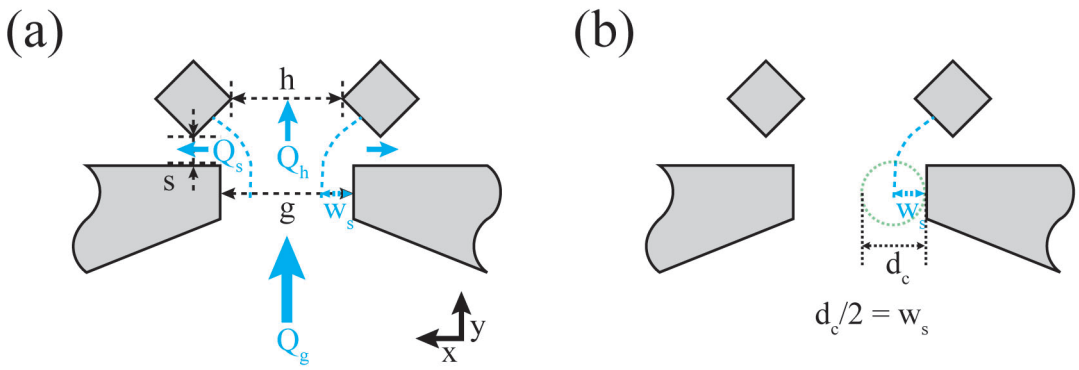

Figure 2.3: The flow division at the trifurcation point of the trap array and critical particle diameter as the width of trapping flow. (a) The flow, Q_g, entering into the inter-barriers gap, g, is divided into three streams: two streams (Q_s) through the trapping gap and a stream (Q_h) through the inter-trapping blocks gap. The dashed blue line is the division line between the flows through each gap. (b) The width (w_s) of the trapping flow is regarded as a half of the critical particle diameter (d_c) for the asymmetric trap/particle interaction. This analysis is based on the qualitative assumption that the contribution of particle surface on streamline calculation is negligible.

The critical particle diameter at given physical dimension was numerically calculated based on the flow profile obtained from FEM (Finite Element Methods) simulation. The array dimension is imported to Comsol® which conducted flow simulation using the fluid mechanics module. After the flow simulation, the flow profile at each gap, inter-barriers gap and trapping gap, is exported. The flow rate at the trapping gap was integrated, and w_s was calculated via an iterative process by using a MatLab code, adjusting the flow rate through w_s at inter-barriers gap until it equals Q_s. It is noteworthy that the probability of error increases as the trapping gap (s) increases because the flow profile at the trapping gap becomes two dimensional, deviating from the mathematical constraint that Q_s is uni-directional.

The line of asymmetry, the critical particle diameter obtained from the theoretical equation, can predict the asymmetric behavior at defined physical dimensions using the geometrical variables. For simplicity, these variables were normalized by the inter-trapping blocks gap: normalized particle diameter (d*=d/h), normalized trapping gap (s*=s/h), and normalized inter-barriers gap (g*=g/h) (Figure 2.4.a). These three parameters determine the value of w_s and, therefore, the fraction of fluid that flows through the trapping region (i.e., through s). The line of asymmetry drawn on a graph of the normalized particle diameter (d*) vs. the normalized trapping gap (s*) indicates the minimum value that the particle motion is still symmetric. Above this line, the trap/particle interaction is asymmetric. Note that the line of asymmetry in this graph shifts when the normalized inter-barrier gap (g*) changed (Figure 2.4.b).

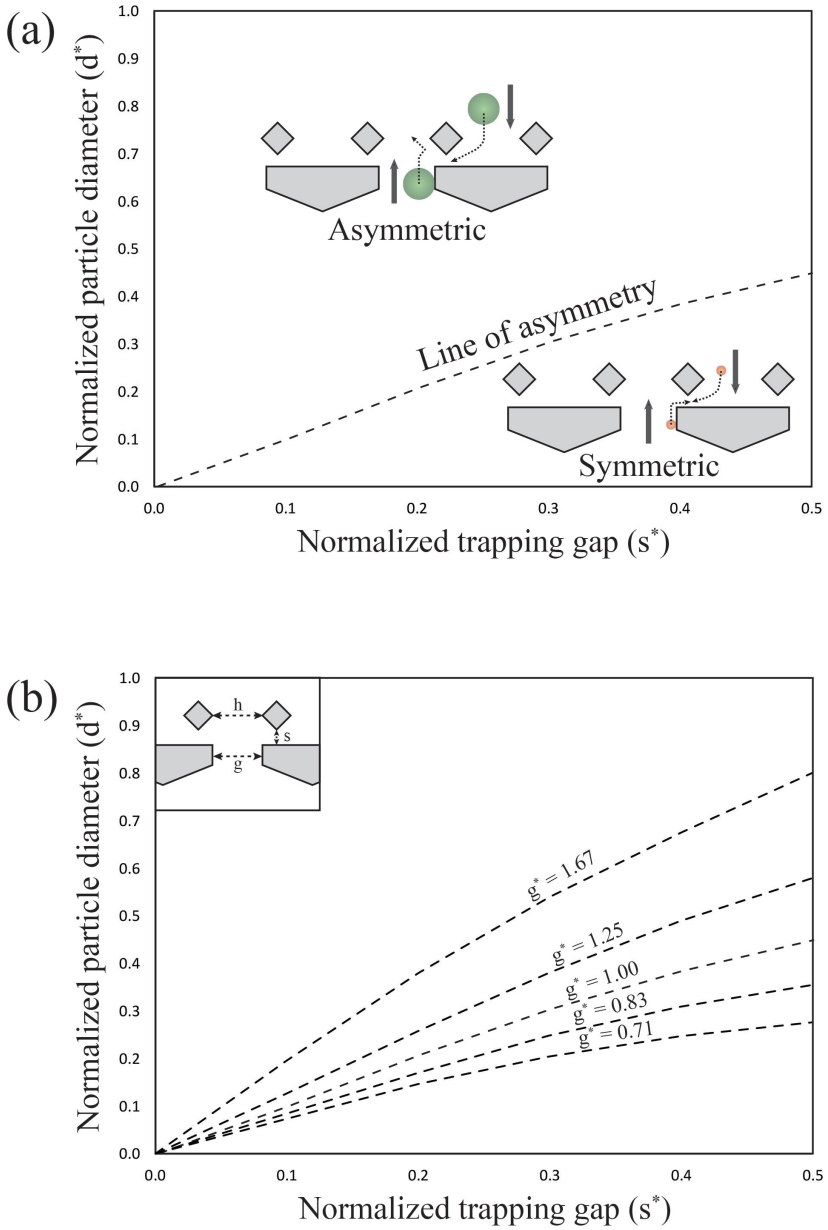

Figure 2.4: The line of asymmetry showing the critical particle diameter in the normalized particle diameter (d*) vs. the normalized trapping gap (s*) graph. The variables with * means the normalization by inter-trapping blocks gap (h). (a) The asymmetric trap/particle behavior, particle passage through only inter-trapping blocks gap (h) during upward flow, happens at the region above the line of asymmetry. In the region below the line of asymmetry, the particle passes through the trapping gap (s). (b) The line of asymmetry shifts as the normalized inter-barriers gap (g*) changes.

2.3.3 Trap/particle interaction regimes

Particles flowing through the system can be captured in two ways. If the particles are larger than the space between repeating units, the particles will not enter the array structure and will merely clog the system (Figure 2.5). The line of channel clogging is the smaller value between unity and the normalized inter-barriers gap (g*). In other words, the normalized diameter of the particle, d*, needs to be less than one and g*. The channel clogging (IV) regime is the area above the line of channel clogging.

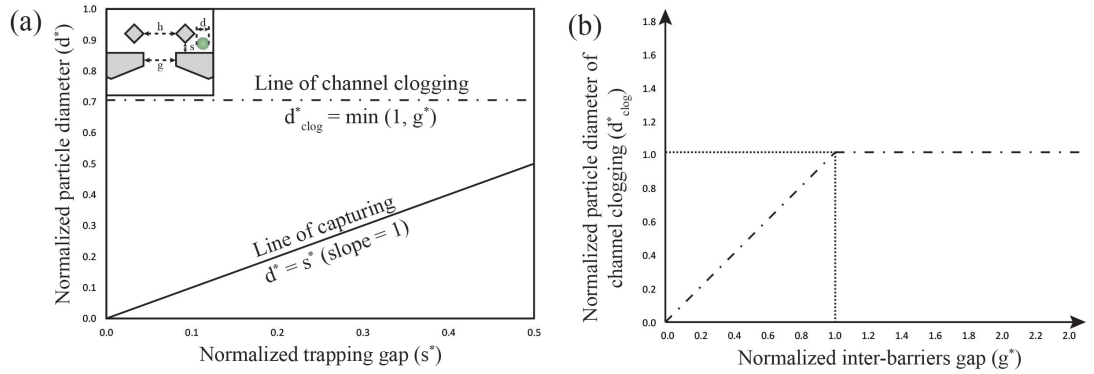

Figure 2.5: Line of capturing and line of channel clogging. (a) The line of capturing means the size of the trapping gap in the graph of normalized parameters. The line of channel clogging means the size of smaller one between inter-trapping blocks gap (h) and inter-barriers gap (g). (b) The size of normalized particle diameter of channel clogging, the line of channel clogging in the graph of normalized parameters, depends on the normalized inter-barriers gap (g*).

The second method of particle capture in the array is by physical trapping in the trapping gap. The values of the normalized particle diameter (d*) and the normalized trapping gap (s*) predict whether the particle will be trapped and what motion will ensue. As can be seen from Figure 2.6, there are 4 different regimes for this trapping or passage: symmetric passage (I), asymmetric passage (IIa), symmetric capturing (IIb), and asymmetric capturing (III) (Figure 2.6). The symmetric passage (I) regime is the area

below both the line of asymmetry and the line of capturing. In this regime, the particle remains on its streamline regardless of the direction of flow, and the particle diameter is small enough not to be captured in the array. The asymmetric passage regime (IIa) is the area above the line of asymmetry and below the line of capturing. Particles in this regime show asymmetric behavior without being captured, which means the particles do not flow through the trapping gap during upward flow, but are able to pass through the trapping gap during downward flow.

As the line of asymmetry shifts by changing the inter-barriers gap, the relative location between the line of asymmetry and the line of capturing inverts. This inversion forms a new area surrounded by the line of asymmetry above and the line of capturing below and is called the symmetric capturing region (IIb). In this region, particles are captured during flow in both directions. This behavior is different than the behavior in the asymmetric capturing (III) regime where particle passage during upward flow and particle capturing during downward flow occur along different streamlines.

The particle flow experiments validated the theoretical trap/particle interaction regimes. As can be seen from figure 2.6, the experimental points lie in the appropriate theoretical sections. The system near the critical lines including the line of capturing and the line of asymmetry showed mixed results of different regimes since both the particles and traps have size distributions. Also, the particles near the sidewall of the channel sometimes behaved differently. For example, the array and particles designed for asymmetric passage (IIa) instead had symmetric passage (I) interaction. This deviation can be attributed to the difference between actual physical dimension of the asymmetric trap at sidewall region and the condition used in the simulation. The geometry used in the

theoretical calculation always had two trapping gaps at both sides of the trap and periodic boundary condition to minimize the effect of the sidewall. However, in the experiments, the trap at the sidewall of the channel has only a single trapping gap causing the deviation from the theoretical results. Another result to be noteworthy is asymmetric behavior of the particles in the symmetric interaction regimes. Since our prediction on the threshold assumes the physical contact between the barrier and a particle, the particles can sometimes show seemingly asymmetric interaction at the symmetric regimes unless the particle is placed on the streamline closest to the barrier of the trap.

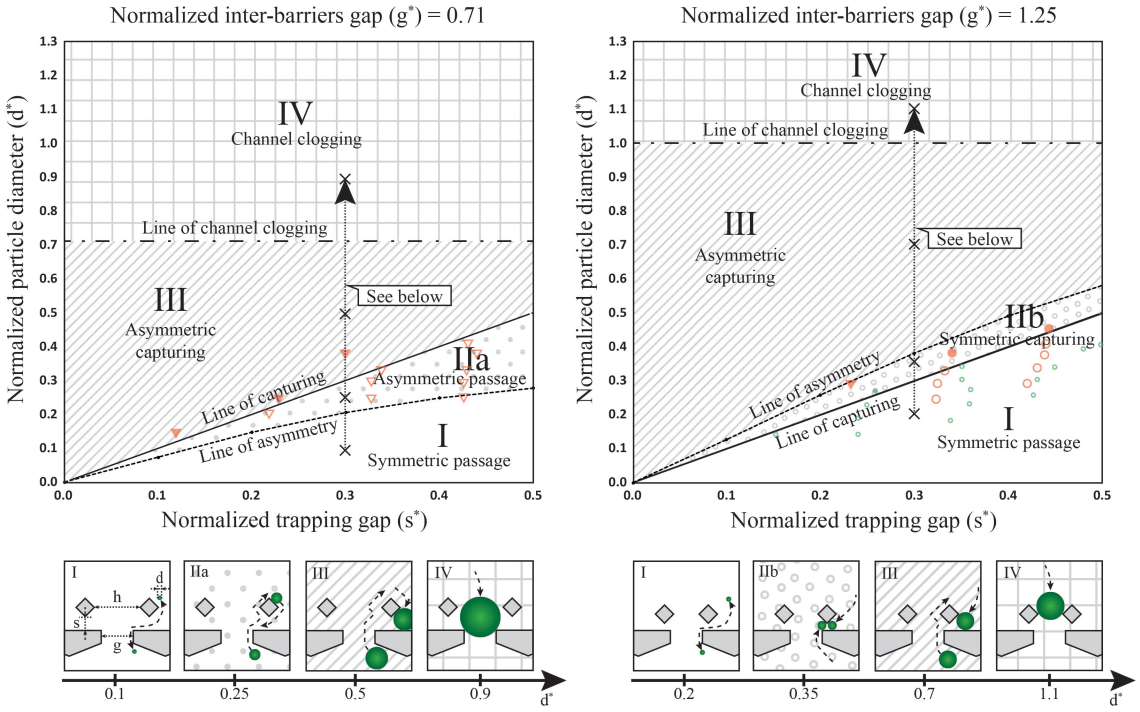

Figure 2.6: Total five different regimes of the trap/particle steric interaction. Three critical lines including the line of asymmetry, the line of capturing, and the line of channel clogging characterize the regimes of trap/particle steric interaction. (Top left) The graph of trap/particle steric interaction regimes at the inter-barriers gap (g*) of 0.71. (Top right) The graph of trap/particle steric interaction regimes at the inter-barriers gap (g*) of 1.25. As the inter-barriers gap (g*) increases from 0.71 to 1.25, the trap/particle interaction characterized by the line of capturing and the line of asymmetry changes from asymmetric passage (IIa) to symmetric capturing (IIb). (Bottom left and right) As the particle diameter (d*) increases at given physical dimension (s* = 0.3) of the trap array, the particle/trap interaction changes from symmetric passage (I) to channel clogging (IV). Each red and green symbol in the graph means experimental validations of the interaction regime: asymmetric capturing (▼), asymmetric passage (▽), symmetric capturing (●), and symmetric passage (○). The color code of the symbol means the size of the particles used in the validation. Red means the particles of 20.3 μm diameter, and green means the particles of 10.1 μm diameter.

2.4 Conclusions

We have demonstrated the construction of the asymmetric trap and its steric interaction with a particle. The threshold of asymmetric behavior in the array of asymmetric traps is theoretically formulated based on mass conservation in a quasi-two-dimensional system. The five different trap/particle interaction regimes including symmetric passage (I), asymmetric passage (IIa), symmetric capturing (IIb), asymmetric capturing (III), and channel clogging (IV) were predicted and experimentally validated. The design guide provided here is applicable for any trap constructed with one large steric barrier and two obstacles for the trapping of particles.

The arrays used in this work usually had relatively low capturing efficiency since we mainly focused on elucidating the principle of the trap/particle interaction. For practical purposes, capturing efficiency can be improved by optimizing the physical dimension of the array. Capitalizing on the asymmetric behavior that originates from the steric interactions, the trap array can perform basic capturing, releasing, and separation of particle suspensions. The direction-dependent capturing behavior of the asymmetric capturing (III) regime can be a useful control variable for those applications. We expect the functionality of trap/particle steric interactions shown in the asymmetric trap array to contribute to easy and flexible manipulation of micron-sized particles.

2.5 References

1. Y. Kang and D. Li, Electrokinetic motion of particles and cells in microchannels, *Microfluidics and Nanofluidics*, 2009, **6**, 431-460.

2. M. D. Vahey and J. Voldman, An equilibrium method for continuous-flow cell sorting using dielectrophoresis, *Analytical Chemistry*, 2008, **80**, 3135-3143.

3. M. A. M. Gijs, F. Lacharme, and U. Lehmann, Microfluidic applications of magnetic particles for biological analysis and catalysis, *Chemical Reviews*, 2010, **110**, 1518-1563.

4. A. Ashkin, Optical trapping and manipulation of neutral particles using lasers, *Proceedings of the National Academy of Sciences of the United States of America*, 1997, **94**, 4853-4860.

5. A. A. Kayani, K. Khoshmanesh, S. A. Ward, A. Mitchell, and K. Kalantar-zadeh, Optofluidics incorporating actively controlled micro- and nano-particles, *Biomicrofluidics*, 2012, **6**, 031501.

6. M. Gedge and M. Hill, Acoutofluidics 17: Theory and applications of surface acoustic wave devices for particle manipulation, *Lab on a Chip*, 2012, **12**, 2998-3007.

7. X. Ding, P. Li, S. S. Lin, S. Stratton, N. Nama, F. Guo, D. Slotcavage, X. Mao, J. Shi, F. Costanzo, and T. J. Huang, Surface acoustic wave micmrofluidics, *Lab on a Chip*, 2013, **13**, 3626-3649.

8. M. Wiklund, R. Green, and M. Ohlin, Acoustofluidics 14: Applications of acoustic streaming in microfluidic devices, *Lab on a Chip*, 2012, **12**, 2438-2451.

9. B. R. Lutz, J. Chen, and D. T. Schwartz, Hydrodynamic tweezers: 1. Noncontact trapping of single cells using steady streaming microeddies, *Analytical Chemistry*, 2006, **78**, 5429-5435.

10. R. I. Zeitoun, D. S. Chang, S. M. Langelier, J. Mirecki-Millunchick, M. J. Solomon, and M. A. Burns, Selective arraying of complex particle patterns, *Lab on a Chip*, 2010, **10**, 1142-1147.

11. K. Chung, C. A. Rivet, M. L. Kemp, and H. Lu, Imaging single-cell signaling dynamics with a deterministic high-density single-cell trap array, *Analytical Chemistry*, 2011, **83**, 7044-7052.

12. D. Di Carlo, L. Y. Wu, and L. P. Lee, Dynamic single cell culture array, *Lab on a Chip*, 2006, **6**, 1445-1449.

13. X. Chen, D. F. Cui, C. C. Liu, and H. Li, Microfluidic chip for blood cell separation and collection based on crossflow filtration, *Sensors and Actuators B*, 2008, **130**, 216-221.

14. S. Faley, Kevin Seale, J. Hughey, D. K. Schaffer, S. VanCompernolle, B. McKinney, F. Baudenbacher, D. Unutmaz, and J. P. Wikswo, Microfluidic platform for real-time signaling analysis of multiple single T cells in parallel, *Lab on a Chip*, 2008, **8**, 1700-1712.

15. S. L. Faley, M. Copland, D. Wlodkowic, W. Kolch, K. T. Seale, J. P. Wikswo, and J. M. Cooper, Microfluidic single cell arrays to interrogate singalling dynamics of individual, patient-derived hematopoietic stem cells, *Lab on a Chip*, 2009, **9**, 2659-2664.

16. L. R. Huang, E. C. Cox, R. H. Austin, and J. C. Sturm, Continuous particle separation through deterministic lateral displacement, *Science*, 2004, **304**, 987-990.

17. D. W. Inglis, J. A. Davis, R. H. Austin, and J. C. Sturm, Critical particle size for fractionation by deterministic lateral displacement, *Lab on a Chip*, 2006, **6**, 655-658.

18. K. J. Morton, K. Loutherback, D. W. Inglis, O. K. Tsui, J. C. Sturm, S. Y. Chou, and R. H. Austin, Hydrodynamic metamaterials: Microfabricated arrays to steer, refract, and focus streams of biomaterials, *Proceedings of the National Academy of Sciences of the United States of America*, 2008, **105**, 7434-7438.

19. D. Di Carlo, Inertial microfluidics, *Lab on a Chip*, 2009, **9**, 3038-3046.

20. A. J. Mach, J. H. Kim, A. Arshi, S. C. Hur, and D. Di Carlo, Automated cellular sample preparation using a Centrifuge-on-a-Chip, *Lab on a Chip*, 2011, **11**, 2827-2834.

21. H. Amini, W. Lee, and D. Di Carlo, Inertial microfluidic physics, *Lab on a Chip*, 2014, **14**, 2739-2761.

22. E. Chmela, R. Tijssen, M. T. Blom, H. J. G. E. Gardeniers, and A. van den Berg, A chip system for size separation of macromolecules and particles by hydrodynamic chromatography, *Analytical Chemistry*, 2002, **74**, 3470-3475.

23. M. Yamada and M. Seki, Hydrodynamics filtration for on-chip particle concentration and classification utilizing microfluidics, *Lab on a Chip*, 2005, **5**, 1233-1239.

24. M. Yamada, M. Nakashima, and M. Seki, Pinched flow fractionation: Continuous size separation of particles utilizing a laminar flow profile in a pinched microchannel, *Analytical Chemistry*, 2004, **76**, 5465-5471.

25. H. Amini, E. Sollier, M. Masaeli, Y. Xie, B. Ganapathysubramanian, H. A. Stone, and D. Di Carlo, Engineering fluid flow using sequenced microstructures, *Nature Communications*, 2013, **4**, 1826.

26. C. Hsu, D. Di Carlo, C. Chen, D. Irimia, and M. Toner, Microvortex for focusing, guiding, and sorting of particles, *Lab on a Chip*, 2008, **8**, 2128-2134.

27. S. L. Stott, C. Hsu, D. I. Tsukrov, M. Yu, D. T. Miyamoto, B. A. Waltman, S. M. Rothenberg, A. M. Shah, M. E. Smas, G. K. Korir, F. P. Floyd, Jr., A. J. Gilman, J. B. Lord, D. Winokur, S. Springer, D. Irimia, S. Nagrath, L. V. Sequist, R. J. Lee, K. J. Isselbacher, S. Maheswaran, D. A. Haber, and M. Toner, Isolation of circulating tumor cells using a microvortex-generating herringbone-chip, *Proceedings of the National Academy of Sciences of the United States of America*, 2010, **107**, 18392-18397.

28. S. Choi and J. Park, Continuous hydrophoretic separation and sizing of microparticles using slanted obstacles in a microchannel, *Lab on a Chip,* 2007, **7**, 890-897.

29. K. Iwai, W. Tan, H. Ishihara, and S. Takeuchi, A resettable dynamic microarray device, *Biomedical Microdevices*, 2011, **13**, 1089-1094.

30. R. D. Sochol, M. E. Dueck, S. Li, L. P. Lee, and L. Lin, Hydrodynamic resettability for a microfluidic particulate-based arraying system, *Lab on a Chip*, 2012, **12**, 5051-5056.

31. R. D. Sochol, S. Li, L. P. Lee, and L. Lin, Continuous flow multi-stage microfluidic reactors *via* hydrodynamic microparticle railing, *Lab on a Chip*, 2012, **12**, 4168-4177.

32. R. D. Sochol, D. Corbett, S. Hesse, W. E. R. Krieger, K. T. Wolf, M. Kim, K. Iwai, S. Li, L. P. Lee, and L. Lin, Dual-mode hydrodynamic railing and arraying of microparticles for multi-stage signal detection in continuous flow biochemical microprocessors, *Lab on a Chip*, 2014, **14**, 1405-1409.

CHAPTER III

ONE-WAY PARTICLE TRANSPORT USING OSCILLATORY FLOW IN ASYMMETRIC TRAPS

3.1 Introduction

Emergence of microfluidics technologies has increased the capabilities of handling micron sized particles. Matching of physical scale and deterministic nature of fluid mechanics at low Reynolds regime enables microfluidic devices to accurately manipulate particles. New passive fluidic techniques such as deterministic lateral displacement, [1,2] inertial microfluidics, [3,4] and pinched flow fractionation [5,6] have been developed by capitalizing on obstacle-particle interactions and fluid flow characteristics including fluid inertia, shear forces, and shaped streamlines. Those techniques proved their abilities to conduct a list of functions including focusing, [7] trapping, [8] and separation [9] of micro-particles with minimal cost of operation. Also, unprecedented capabilities such as the recovery of circulating tumor cells (CTCs) from blood based on size or deformability difference [10,11] and high throughput mechanical characterization of a single cells [12-15] have been demonstrated.

In addition to the physical properties of particles and fluid flow, time dependent variation of a flow field, e.g. oscillation of fluid flow, is another factor that can add

unique processing capabilities to passive fluidic techniques. Parametric pumping [16-18] is a good example of effective use of oscillatory flow. In parametric pumping, oscillatory flow synchronous with temperature cycles of a packed column enables the enhanced transport of a target solute. The column uses the repetition of a two-step cycle that consists of adsorption at low temperature and desorption at high temperature to accomplish this feat. Very high separation factors as large as 10^5:1 can be achieved by focusing desorbed target solutes into specific areas.

Likewise, oscillatory flow can be used in microfluidic operations to enhance or modify the transport of particles. The oscillatory operation can be conducted in a batch mode, and this closed fluidic circuit allows a multi-step process to be sequentially implemented in segmented batches. This type of operation removes the operational restraints found in continuous system and allows any error in a processing step to be mitigated, an option that is difficult in continuous systems. [19] Incorporation of passive fluidic techniques could reduce complexity in the design and implementation of integrated devices by removing peripheral systems that accompany active techniques such as magnetophoresis, [20-25] dielectrophoresis, [26-32] acoustophoresis, [33-36] and optical tweezers. [37,38]

In Chapter 2, we analyzed the steric hindrance to induce flow direction-dependent variations in trap-particle interactions. [39] The asymmetric trap allows the capturing of particles in one flow direction and no capturing of particles in the opposite direction. We modeled the trap-particle interactions based on geometric parameters of the traps and the diameter of the particles, and the model could successfully predict experimental observations. However, our investigation on the interactions was limited to a single row

of asymmetric traps under a continuous flow. The particle dynamics in oscillatory flow across multiple rows of asymmetric traps was not studied.

Here, we report on a passive fluidic technique, one-way particle transport, for micro-particle manipulation in oscillatory flow at low Reynolds numbers ($Re < 0.01$). This transport technique displaces micro-particles in only one direction in oscillatory flow by capitalizing on interactions between micro-particles and the asymmetric traps. To the best of our knowledge, there has been only a single work that showed irreversible transport of micro-particles in oscillatory flow field. [40] While that work solely depends on hydrodynamic transport of the particles, our particle transport uses mechanical capturing to achieve a net displacement of micro-particles in oscillatory flow. We defined four conditions necessary to achieve one-way particle transport and verified these conditions theoretically and experimentally. The four conditions are: mechanical capture, asymmetric interaction, physical collision, and lateral shift, and we estimated the critical particle diameters to obtain each of those four conditions. These critical particle diameters provided predictions on the type of trap-particle interactions that were favorably matched with experimentally observed particle dynamics. These results imply that the combination of trap-particle interactions in the asymmetric traps can produce unique operations such as separation and focusing of micro-particles.

3.2 Material and Methods

3.2.1 Numerical methods

FEM (Finite Element Method) simulation and numerical calculation were used to calculate the critical particle diameters and the location of the boundary streamlines of

the capturing stream. The asymmetric traps were drawn by L-Edit (v.12.11), and the geometry file was imported to COMSOL Multiphysics®. Detailed information on the array dimension is provided in the Appendix A. To obtain flow profiles at each gap of the trap array, the fluid mechanics module was used. No-slip boundary condition was applied to the boundary of the traps and periodic boundary condition was applied to the sidewall of the system to minimize the effect of channel wall on the flow profile (Appendix B). The flow profiles from FEM simulation was used in MATLAB® to calculate the critical particle diameters and the location of the boundary streamlines based on the mass balance equations that was analytically formulated. The correction factor η was obtained by counting the number of streamlines that shift through gaps and the number of streamlines at inter-barriers gap (g).

3.2.2 Fabrication of the microfluidic device

The device had three layers including fluidic channel layer, control channel layer on top, and thin polydimethylsiloxane (PDMS) membrane separating the first two layers. The fluidic channel of the device was constructed by photolithography and dry etching process of Si wafer. A photoresist (SPR 955CM, Microchem Corp.) was spin-coated at 3000 rpm on a Si wafer. After a pre-bake for 1 min at 100 ^{o}C on a hot plate, the photoresist was exposed for 5 sec (30 mJ/cm^2) by a mask aligner (MA/BA6 mask aligner, Karl Suss MicroTec). The pattern was post-baked for 1 min at 110 ^{o}C on a hot plate, and was developed (AZ® 726, MicroChemicals). Following deep reactive ion etching (DRIE) (STS Pegasus 4, SPTS Technologies, Ltd.) built fluidic channel and posts. Control channel was made micromolding of PDMS on a mold made of Si. The Si mold of 100 μm depth was shaped by photolithography and DRIE as done for the fluidic channel. The

surface of the Si mold was coated with a trichlorosilane ((tridecafluoro-1,1,2,2-tetrahydrooctyl)-1-trichlorosilane, UCT) for surface passivation. The PDMS monomer and cross-linker were mixed as 10:1 (w/w) ratio. The mixture was poured on the Si mold, and was degassed before the curing at 80 ^{o}C for 1.5 hr in an oven. The thin membrane between fluidic channel and control channel was made by spin-coating and curing. The PDMS mixture was prepared as done for control channel, and spin-coated at 600 rpm on a Si wafer after degassing of the mixture. The PDMS film on the wafer was cured at 140 ^{o}C for 3 hrs on a hot plate. Prepared parts including fluidic channel, control channel, and thin film were plasma-bonded to each other. It should be noted that the area of normally-closed valves in both the fluidic channel and the control channel were masked by PDMS blocks during plasma treatment.

3.2.3 Experimental validation of one-way particle transport

Before use, the device was primed with buffer solution, a mixture of deionized water, OptiPrep^{TM} density gradient medium (Sigma-Aldrich Co.), and Tween 20 surfactant (Sigma-Aldrich Co.). The density of the buffer was equivalent to it of the micro-particles. The inlets of the primed device were connected to pneumatic pressure/vacuum lines. The vacuum opened normally-closed valves, and the buffer containing particles (mean diameter = 20.3 μm, Spherotech, Inc.) was injected. When the loading of the particles was finished, all of the valves were closed by pressure. Following cyclic opening of solenoid valves linked to two actuation membranes achieved oscillatory flow across the array region. The motion of particles were recorded by a ccd camera (Grasshopper$^{®}$3, Point Grey Research, Inc.) mounted on the top of a stereo microscope (SZX12, Olympus Corp.).

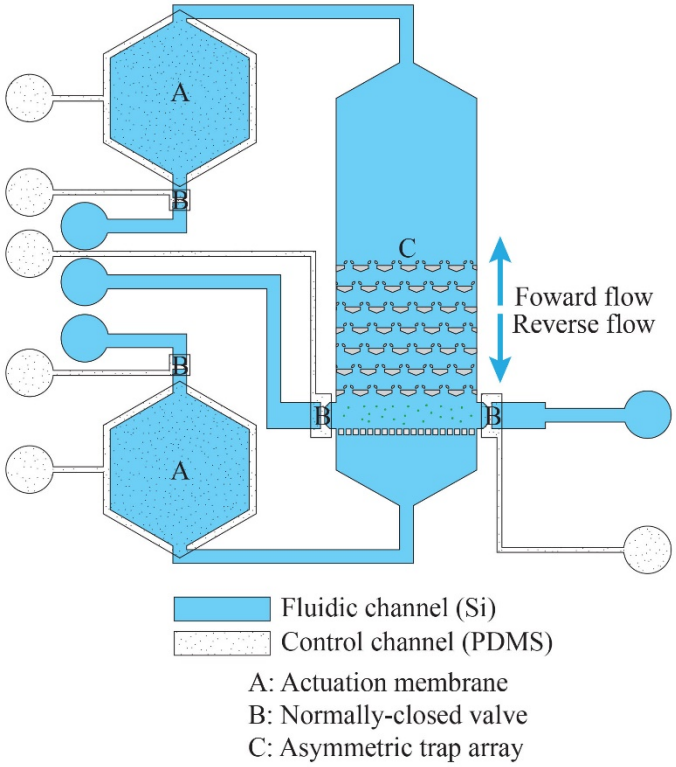

Figure 3.1: Device diagram. The device consists of three layers including bottom fluidic channel, top control channel, and thin PDMS membrane separating two channels.

3.3 Results and discussion

3.3.1 One-way particle transport

One-way particle transport — a positive net displacement of the particle without any net fluid motion — can occur in asymmetric traps in oscillatory flow (Figure 3.2). During flow in the forward direction, the particles flow around traps without being captured due to the steric trap-particle interaction.[39] When the flow is reversed, the particles are mechanically captured by asymmetric traps. The traps that capture the particles are located above the initial positions of those particles, resulting in a net positive displacement of the particles after each fluid oscillation. The fluid, on the other

hand, and any other non-capturing particles have a zero net displacement. The repetition of this trap-and-release interaction transports the particles to the end region of the asymmetric traps.

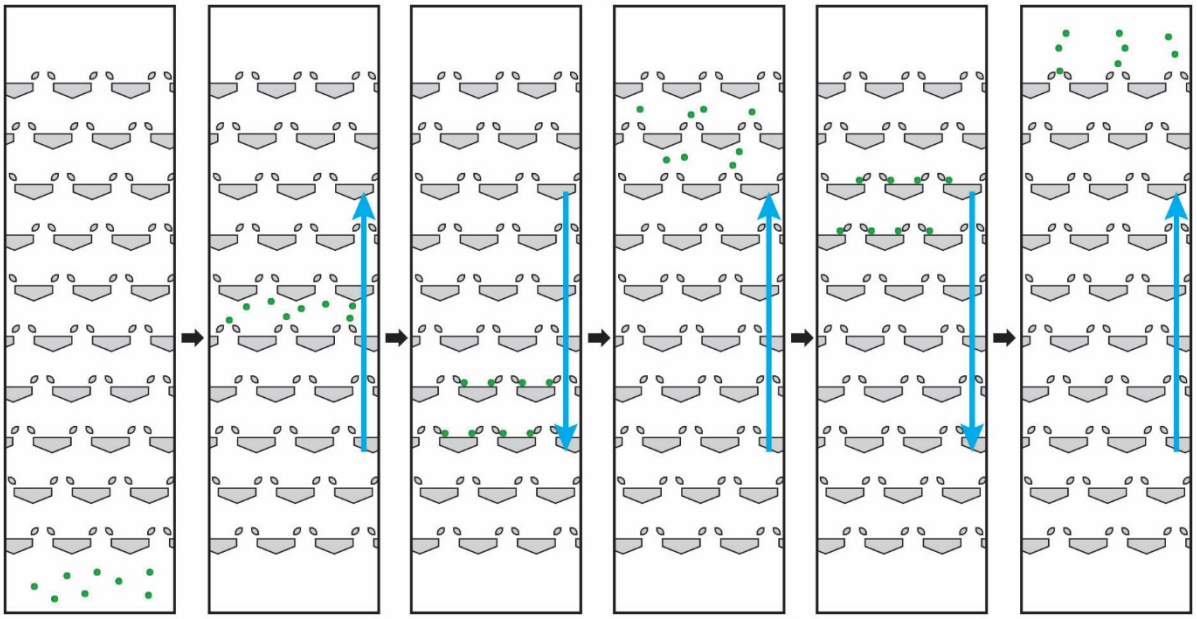

Figure 3.2: One-way particle transport in oscillatory flow. The repetition of passage-capture trap/particle interaction leads to positive net displacement in the oscillation of the fluid, which has a zero net displacement.

Particle capturing in an asymmetric trap is based on mechanical filtering of the particles. A particle is trapped in an asymmetric trap if its diameter is greater than the size of the trapping gap, s (Figure 3.3.a). The critical particle diameter, d_{cap}, is the minimum diameter of particles that will be captured by the trap, which is equivalent to the size of the trapping gap. Figure 3.3.b shows d_{cap} on a plot of the normalized particle diameter, d^* vs. the normalized trapping gap, s^*. Notation "*" denotes normalization of the variable by dividing it by the inter-trapping blocks gap, h. If the particle diameter is larger than the d^*_{cap} line drawn in the graph, the particle will be mechanically filtered by the trap.

An important point to note is that the particle must move asymmetrically to be transported through the asymmetric trap array in oscillatory flow. The asymmetric motion of the particle around the trap during forward flow only occurs if the particle size is greater than the critical particle diameter for asymmetric interaction, d^*_{asymm}. If the diameter is less than this d^*_{asymm}, the particle will be trapped in both forward and reverse flow, and experiences no net displacement. d^*_{asymm} can be estimated, as previously reported, by using a mass balance relationship of flow streams in the trifurcation point at a space between two asymmetric traps.[39] At this trifurcation point, a fraction of the flow at the inter-barriers gap, g, flows into the trapping gap, leading the particle to the trapping region. If particle radius is greater than the width of the flow, w_{asymm}, the particle avoids getting trapped in forward flow (Figure 3.3.c). As shown in Fig. 3.2.d, if the particle diameter is greater than d^*_{asymm}, which was obtained by numerically solving the mass balance relationship, the trap/particle interaction becomes asymmetric and the particle flows around the trap during forward flow. Note that the streamlines will be affected by the presence of particles and variation in the dimensions of the gaps and will, therefore affect this calculation. However, this technique provides a simple and convenient way to estimate the critical particle diameter with acceptable accuracy across a range of gap sizes and particle diameter.

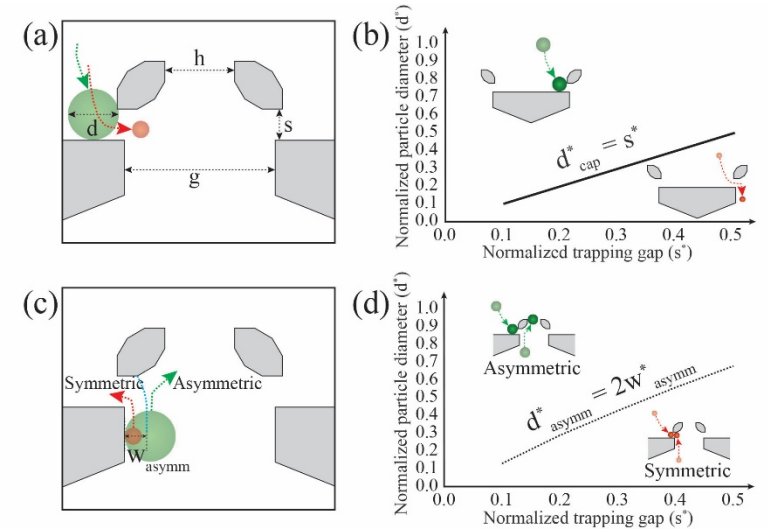

Figure 3.3: The mechanical capturing and asymmetric trap-particle interaction. (a) The particle (green) with the diameter greater than trapping gap, s, is mechanically captured. Otherwise, the particle (red) passes through the trapping gap. (b) The critical particle diameter, d^*_{cap}, for mechanical capturing is equivalent to the trapping gap, s^*. (c) If the radius of the particle is greater than w_{asymm}, the particle shows the asymmetric interaction, which allows the particle to pass the trap array during forward flow. (d) Calculated critical particle diameter, d^*_{asymm}, for the asymmetric interaction. If the particle diameter at a given sizes of trap gaps is above d^*_{asymm}, the trap-particle interaction becomes asymmetric. The superscript "*" denotes the normalization by the inter-trapping blocks gap (h).

3.3.2 Physical collision to overcome reversibility

Physical collision between the asymmetric trap and the particle is essential to overcome hydrodynamic reversibility in oscillatory flow at low Reynolds number (i.e., Re < 0.01). This hydrodynamic reversibility causes a particle transported forward to come back to the initial position via the same path in oscillatory flow, preventing a net displacement (Figure 3.4.a). Physical collision of the particle with the trapping blocks of the asymmetric traps laterally shifts the particle onto a different streamline. The new streamline flows into a trapping gap further forward of the initial location of the particle, and the eventual capture in reverse flow results in a net forward displacement of the particle (Figure 3.4.b).

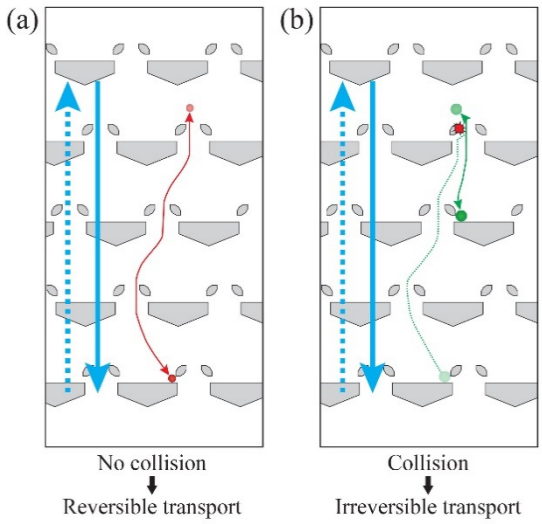

Figure 3.4: Physical collision to overcome hydrodynamic reversibility. (a) Without a physical collision during forward flow, the particle returns to its initial position so that no net displacement occurs. (b) The collision between a particle and a trapping block can induce lateral shift of the path of the particle, causing irreversible transport that results in positive net displacement.

The critical particle diameter, d_{col}, for having this physical collision is obtained based on an analysis of the flow splitting phenomena in the periodic obstacle array and the mass balance relationships between the flow streams. Flow through the periodic obstacles can be described by a number of unit flows, Q_{unit}, that cyclically change their relative positions at inter-barriers gaps (Figure 3.5.a). A particle whose size is relatively small compared to the inter-trapping blocks gap is thought to follow one of the unit flows as a zig-zag mode of transport.[41] The collision probability of the particle in the zig-zag transport is highest when the particle is in a unit flow closest to the sides of the inter-trapping blocks gap (Figure 3.5.b). If the diameter of the particle is greater than the width of the unit flow, w_{uh}, at the inter-trapping blocks gap, at least a single collision is guaranteed at every vertical period of the array (Figure 3.5.c). Otherwise, the particle can pass through a period of the array without a collision. Note that the number of unit flows is generally given as $1/(\varepsilon\eta)$ where ε is the row shift fraction that decides the periodicity of the array and η is a ratio, normalized by ε, of a unit flow to total flow in the inter-barriers

gap. This η is a calibration factor for the asymmetric traps that have small vertical spacing.

If the system is assumed to be two dimensional, d_{col} can be regarded as the width, w_{uh}, of the unit flow at the inter-trapping blocks gap, h.

$$d_{col} = w_{uh} \tag{1}$$

w_{uh} can be estimated by using a mass balance between Q_{unit}, Q_s, and rest of the flow stream flowing through w_{uh} in the gap h (Figure 3.4.d).

$$Q_{unit} - Q_s = \int_0^{w_{uh}} v_h dh \tag{2}$$

In Equation 2, v_h is forward velocity of the flow at the h. It should be noted that only cases where $Q_{unit} > Q_s$ are considered for practical purpose. FEM simulations showed Q_{unit} is greater than Q_s for all of the tested geometries (ε = 1/5, 1/4, 1/3, and 1/2, and $0.1 \leq s^* \leq 0.5$). The opposite case, $Q_{unit} < Q_s$, at small ε such as 0.01 could also have a physical collision, but it is impractical for actual use due to the large numbers of trap rows.

The d^*_{col} was found to be approximately the row shift fraction, indicating that a particle with d^* greater than the row shift fraction is likely to have a physical collision (Figure 3.4.e). This result can be attributed to the splitting of Q_{unit} at the trifurcation point and the parabolic flow profile in the gaps. The parabolic flow profile in the gap between trapping blocks necessitates that the width of the Q_{unit} located near the blocks is larger than the Q_{unit} in central region, increasing w^*_{uh} to a value above an even division (i.e., greater than εη). As the trapping gap increases, the Q_s that stems from Q_{unit} decreases w^*_{uh}. For trapping gaps of 0.2-0.5, η is approximately one so that w^*_{uh} and d^*_{col} are close to the row shift fraction. For a trapping gap of 0.1, w^*_{uh} is below the row shift fraction ($w^*_{uh} \sim 0.31 < \varepsilon \sim 0.33$), which is attributable to a reduced Q_{unit} that counteracts the effect of

the decreased trapping gap. It should be noted that, as shown in the Appendix A, vertical spacing of the trap rows was designed to be proportional to the height of the asymmetric trap for the purpose of minimizing the variation of Q_{unit}. The decreased spacing of the trap rows for the trapping gap of 0.1 reduces Q_{unit}, which is shown as a reduced calibration factor (η~0.75).

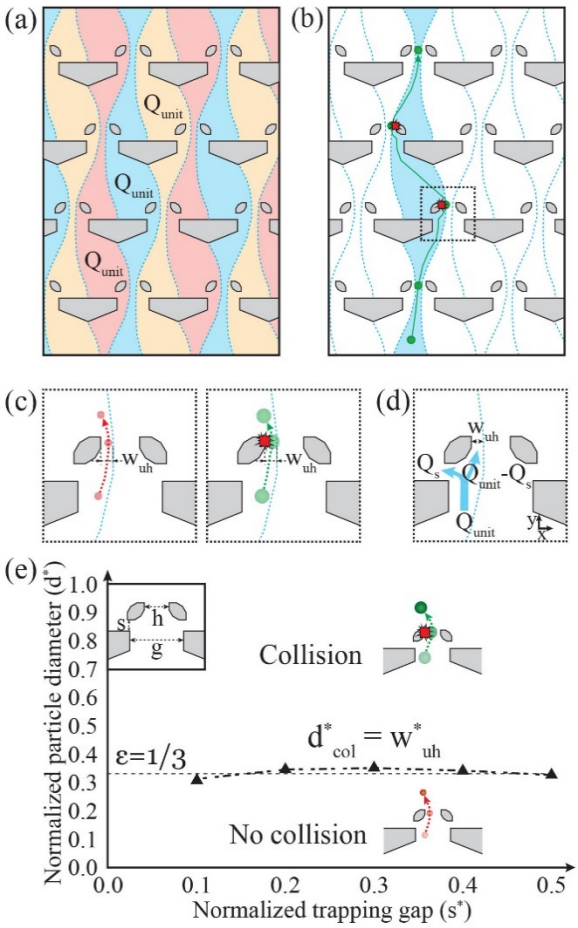

Figure 3.5: The critical particle diameter, d^*_{col}, for having at least a single physical collision during forward transport through a vertical period of the asymmetric traps. (a) The flow in the periodic obstacles splits into a number of unit flows, Q_{unit}, distinguished by colors. (b) While following one of the unit flows, the particle is likely to collide onto a trapping block when the unit flow is located at the sides of inter-trapping blocks gap. (c) The particle having greater size than the width, w_{uh}, of Q_{unit} at inter-trapping blocks gap collides onto a trapping block. Otherwise, the particle can flow through the inter-trapping blocks gap without the physical collision. (d) Mass balance relationship to estimate w_{uh}. (e) The calculated d^*_{col} based on the mass balance relationship. d^*_{col} is around 1/3, the row shift fraction (ε) of the asymmetric traps used here.

3.3.3 Lateral shift into capturing stream

The capturing of particles during reverse flow is predictable based on the deterministic lateral shift of the particles and the periodicity of the fluid flow in the trap array. The particle in reverse flow passes the inter-trapping block gap of each row until it is captured. When the particle flows down a row, the lateral position of the particle in the gap is deterministically changed by the fluid flow across the array and the physical collisions discussed previously. While being laterally shifted during reverse transport, the particle is captured if its center is placed into a capturing stream, the fluid stream passing through the trapping gaps of an asymmetric trap, as shown in Figure 3.6. This capturing stream exists in every inter-trapping blocks gap due to the periodic configuration of the array. By finding the distance of the lateral shift and exact location of the capturing stream, the capturing of the particles can be predicted.

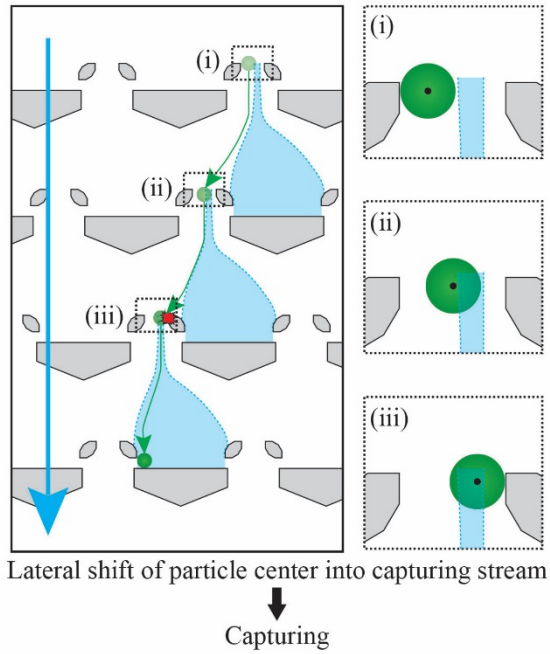

Figure 3.6: Lateral shift of the particle into the capturing stream (blue area) during reverse flow. While the lateral location of the particle in the inter-trapping blocks gap changes from (i) to (ii) and to (iii), the particle is transported to the trap once its center (shown as a black dot) is placed in the capturing stream.

Three rules dictate the lateral shift of the particle in the inter-trapping blocks gap during reverse flow. First, the particle in the beginning of reverse flow is located at the lateral position aligned by the physical collision with the trapping block during the previous forward flow (Figure 3.7.a). Second, traveling down a row of the asymmetric traps, the particle is laterally shifted by w_{uh} due to a unit flow (Q_{unit}) (Figure 3.7.b). It should be noted that the lateral shift made by Q_{unit} moves in only one direction because of the direction of the row shift of the asymmetric traps. Third, the distance of the lateral shift is limited by the size of the inter-trapping blocks gap. In other words, after a series of lateral shifts, the particle collides with a trapping block on the opposite side of the inter-trapping blocks gap (Figure 3.7.c). Based on these rules of deterministic lateral shift, the lateral location of the particle in the inter-trapping blocks gap during reverse flow can be tracked.

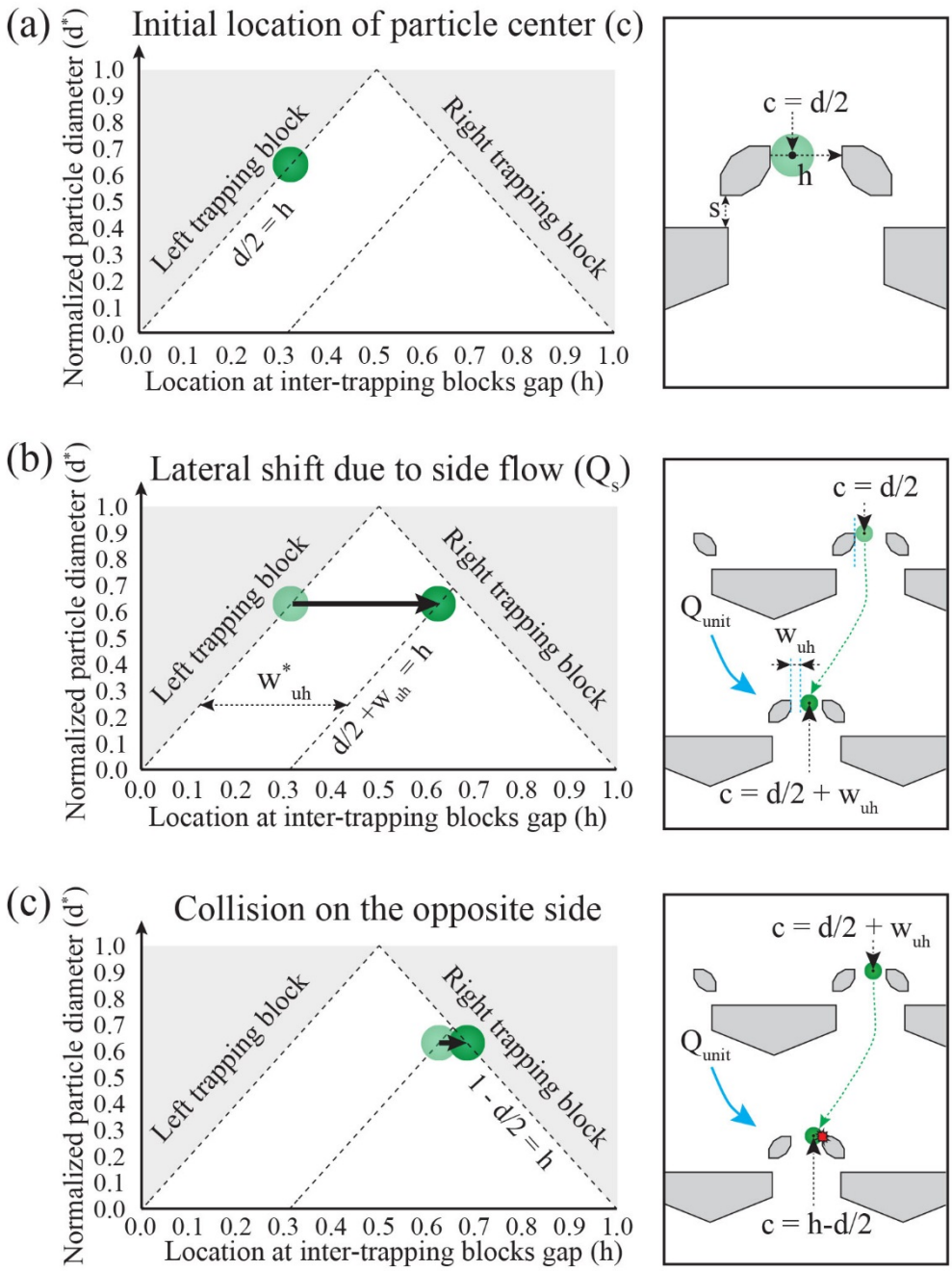

Figure 3.7: Three rules of deterministic lateral shift of the particle during reverse flow. (a) The initial position of the particle in the beginning of reverse transport. The particle is aligned by a trapping block on which the particle collided in the previous forward flow. The initial position of the particle in reverse flow depends on the size of the particle because the distance of the shift made by the physical collision depends on the diameter of the particle. (b) The lateral shift made by unit flow (Q_{unit}). The distance of the shift is equals to the width of the unit flow at the inter-trapping blocks gap. (c) Limit of the lateral shift. After subsequent lateral shifts, the particle collides onto a trapping block on the opposite side, which becomes the limit of the lateral shift.

The location of the capturing stream can be determined by finding boundary streamlines of the capturing stream based on mass balance relationships of the flow streams across two rows of asymmetric traps (Figure 3.8). The region of the capturing stream is defined by b_l and b_r, where b_l is the leftmost streamline that enters the trapping gap and b_r is the rightmost streamline. The location of b_l and b_r can be found by using three mass balance relationships. First, the volumetric flow rate of the capturing stream is equal to the total volumetric flow rate of the flows through two trapping gaps of an asymmetric trap (Figure 3.8.b).

$$Q_{bl} - Q_{br} = 2Q_s \tag{3}$$

where Q_{bl} is the volumetric flow rate of the flow through the region between the b_l and the right trapping block, Q_{br} is the volumetric flow rate of the flow through the region between the b_r and the right trapping block, and Q_s is the volumetric flow rate through the trapping gap. Second, Q_{unit} is equal to the sum of Q_{br} and $2Q_s$ merged during reverse flow (Figure 3.8.c).

$$Q_{br} + 2Q_s = Q_{unit} = \eta \epsilon Q_g \tag{4}$$

It should be noted that the above equation (4) is modified in the case of $2Q_s \geq Q_{unit}$ (Appendix C). Finally, by examining the trifurcation point between two asymmetric traps (Figure 3.8.d), we see that the flows from the inter-trapping blocks gap and two trapping gaps merge into a flow through the inter-barriers gap.

$$2Q_s + Q_h = Q_g \tag{5}$$

where Q_h is volumetric flow rate of the flow through the inter-trapping blocks gap. The above three mass balance equations can be transformed into two equations for Q_{bl} and Q_{br} shown below.

$$\frac{Q_{bl}}{Q_h} = 2\eta\epsilon\frac{Q_s}{Q_h} + \eta\epsilon \tag{6}$$

$$\frac{Q_{br}}{Q_h} = -2(1-\eta\epsilon)\frac{Q_s}{Q_h} + \eta\epsilon \tag{7}$$

Q_{bl} and Q_{br} are linked to the location of b_l and b_r at the inter-trapping blocks gap through the mathematical definitions of Q_{bl} and Q_{br}

$$Q_{bl} = \int_{bl}^{1} v_h dh \tag{8}$$

$$Q_{br} = \int_{br}^{1} v_h dh \tag{9}$$

The location of the boundary streamlines was found to be around a point at 1-w_{uh} of the inter-trapping blocks gap with increasing distance between the streamlines at greater trapping gap values (Figure 3.8.e). The locations of b_l and b_r at various trapping gap sizes (0.1-0.5) were numerically calculated. b_l and b_r should merge into the boundary line of Q_{unit}, 1-w_{uh} of the inter-trapping blocks gap, at zero trapping gap because half of the flow stream between b_l and b_r belongs to Q_{unit}. As the trapping gap increases, b_l and b_r move away from the boundary line of Q_{unit}.

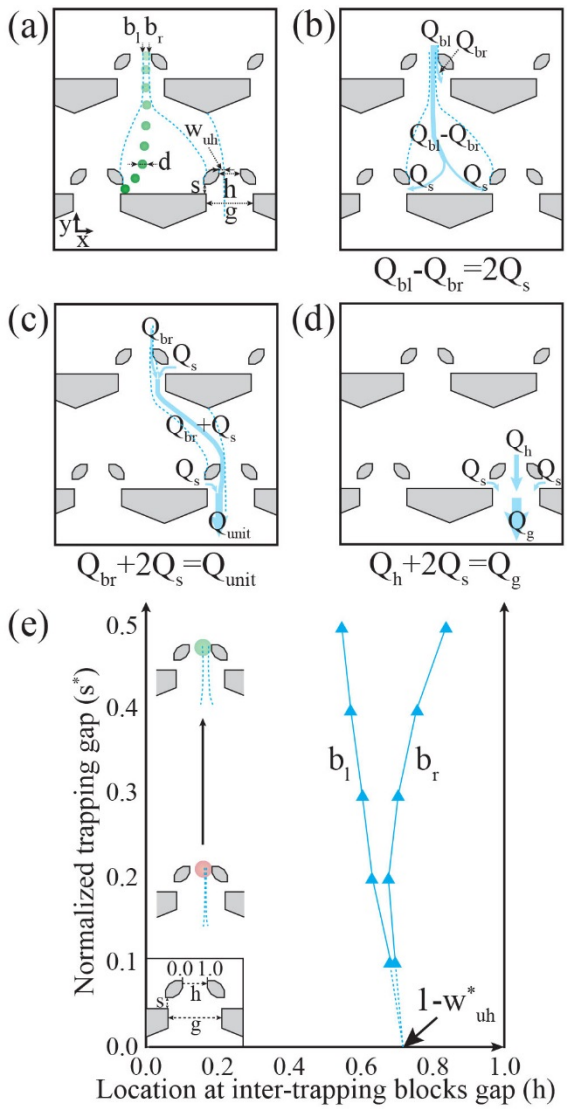

Figure 3.8: The locations of boundary streamlines, b_l and b_r, of the capturing stream at the inter-trapping blocks gap. (a) Only the particle whose center is located between b_l and b_r is captured during reverse flow. (b–d) The diagrams showing mass balance relationships between flow streams for finding the location of b_l and b_r. Q_{bl} and Q_{br} are the flow rates in the region between b_l and a trapping block on the right, and b_r and the trapping block on the right, respectively. (e) The location of b_l and b_r at inter-trapping blocks gap. The row shift fraction is 1/3. As the normalized trapping gap increases, the distance between b_l and b_r increases due to increased amount of the capturing stream.

The capturing behavior of a particle can be predicted by comparing the lateral location of the particle during reverse flow and the location of the capturing stream in the inter-trapping blocks gap. In Figure 3.9.a, the lateral location of three different sized particles during reverse flow and the location of the capturing stream, defined by the

boundary streamlines, are drawn in a single graph. For this graph, if the center of the particle enters into the region of the capturing stream (i.e., the region between b_l and b_r), then the particle is captured in the next row. For the large particle ((i) in Figure 3.9.a), a single lateral shift results in contact with the opposite trapping block. The particle center remains outside of the capturing stream and the particle cannot be captured. For the next largest particle ((ii) in Figure 3.9.a), a single lateral shift results in a collision with the opposite trapping block but this new position is now in the capturing stream and the particle is captured after flowing down a row of the asymmetric traps. For the smallest particle ((iii) in Figure 3.9.a), both the first and second lateral shifts result in the particle being outside the capturing stream and, like the largest particle, this particle cannot be captured. The diameter range for the lateral shift into the capturing stream was calculated for different trapping gap sizes (0.1-0.5) (Appendix D), and the results were merged into a single graph of normalized particle diameter and normalized trapping gap (Figure 3.9.b). Note that only the particles with diameters greater than d^*_{cap} can be captured, as described previously.

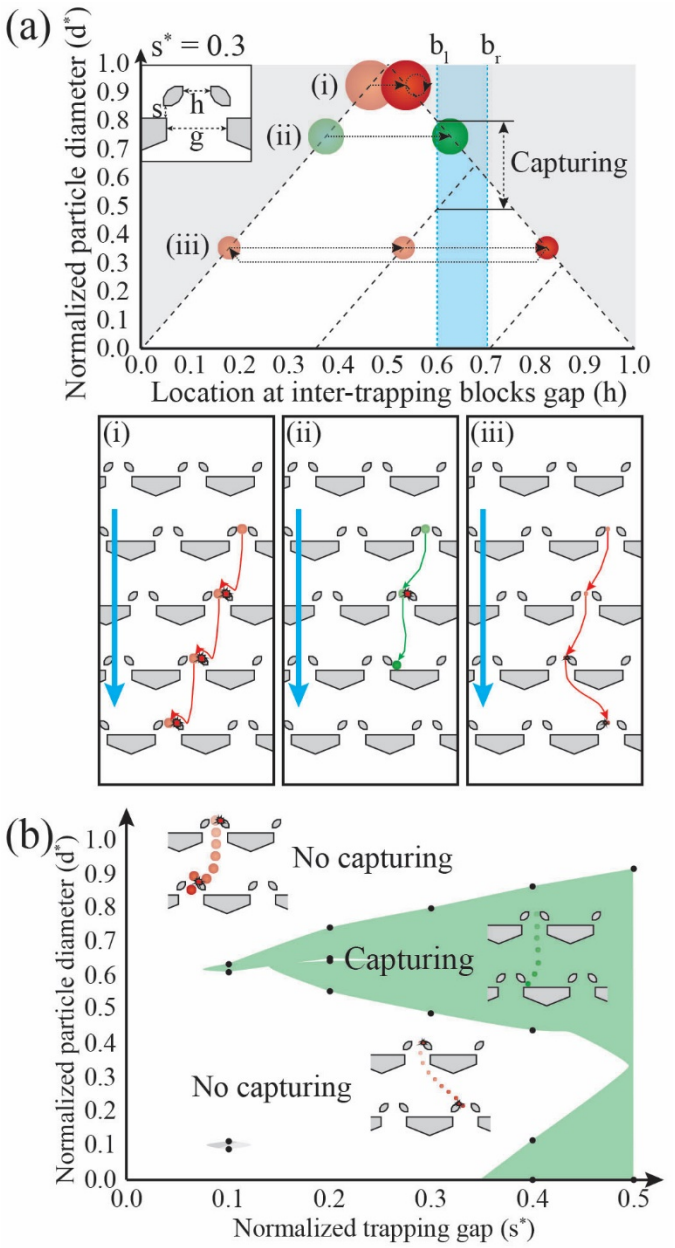

Figure 3.9.: Prediction of the capturing based on the combination of deterministic lateral shift of the particle and the location of the capturing stream. (a) Only the particle whose center enters the capturing stream is captured during reverse flow. The location of the capturing stream at given trapping gap size ($s^* = 0.3$) was shown as blue shaded region between b_l and b_r. After the particle reaches to the other side of the inter-trapping blocks gap, the particle either keeps its lateral position (large particles which show the bump mode transport) or goes back to initial lateral location (small particle which shows the zig-zag mode transport). (b) The diameter range of particles for capturing at given trapping gap sizes (0.1-0.5) was calculated. Black dots are calculated intersections between the location of the boundary streamlines and line of lateral locations of the particle center. At given dimensions of the array, only the particle in the shaded region has a chance of deterministic capturing. It should be noted that the line between the calculated points were interpolated based on the trend of diameter range at two trapping gap sizes.

3.3.4 The dimension and oscillation amplitude for one-way particle transport

To implement one-way particle transport, all the conditions of the trap-particle dynamics previously discussed should be satisfied. The array dimension for one-way particle transport can be easily found by combining the graphs of the critical particle diameters d^*_{cap} for mechanical capturing, d^*_{asymm} for the asymmetric interaction, d^*_{col} for having a physical collision, and the diameter for the lateral shifting into a capturing stream (Figure 3.10). Thus, for a given array, the particles that are laterally shifted into the capturing streams (green region in Figure 3.10) can achieve one-way particle transport if their diameter satisfies $d^* \geq \text{Max}\,[d^*_{cap}, d^*_{asymm}, d^*_{col}]$. In Figure 3.10, those d^* values are shown as dark green.

The phase diagram suggests that the maximum range of particle diameter for one-way particle transport is at a medium trapping gap ($s^* \sim 0.34$) (Figure 3.10). This, in turn, suggests that a particle would reliably achieve one-way particle transport with its widest range of diameters at a trapping gap of approximately 1/2 the average particle diameter and an inter-trapping blocks gap of approximately 3/2 the average particle diameter. As the trapping gap increases, the range of d^* for entering into the capturing stream widens, but the increase of d^*_{asymm} counteracts this effect. The trade-off of these two factors is why the range of particle diameters for one-way particle transport has its maximum value at medium trapping gap. The phase diagrams of different row shift fraction (ε = 1/5, 1/4, and 1/2) show similar trends (Appendix E).

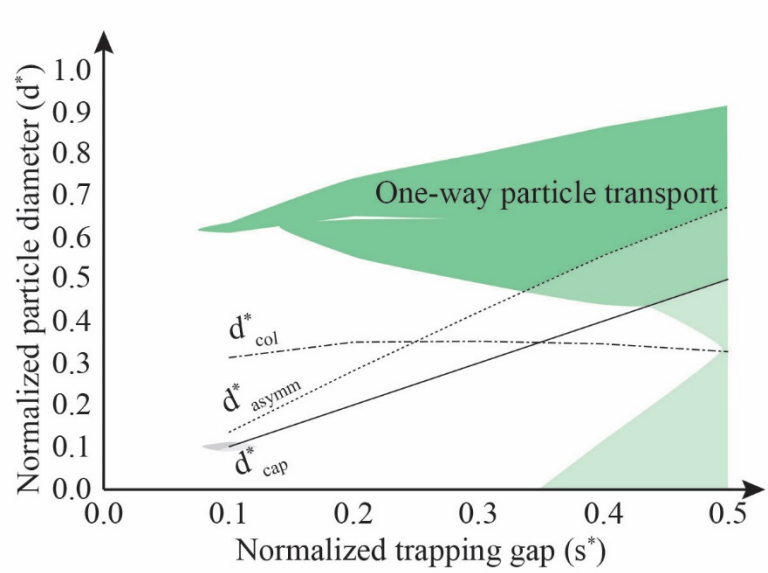

Figure 3.10: The dimensions for the one-way particle transport. The particles should satisfy the conditions including mechanical capture ($d^* \geq d^*_{cap}$), asymmetric interaction ($d^* \geq d^*_{asymm}$), physical collision ($d^* \geq d^*_{col}$), and lateral shift into a capturing stream (d^* belonging to the shaded region in Figure 3.9.b). The dark green shaded region here satisfies all of those conditions. The row shift fraction of the array is 1/3, and the ratio of inter-trapping blocks gap, h, to inter-barriers gap, g, is 1.5.

In principle, an oscillation amplitude, λ, greater than two vertical periods of asymmetric traps is necessary for one-way particle transport. The amplitude of the fluid oscillation should be large enough to provide the possibility of capture during reverse flow (Figure 3.11.a). Although the minimum amplitude for one-way particle transport varies with particle diameter, a convenient way to determine the amplitude is to have the amplitude greater than two vertical periods, the distance of 2/ε rows, of asymmetric traps (Figure 3.11.b). Since the particles are captured while passing across a single period, 1/ε rows of traps, and taking into account that no collisions occur in the region where the array changes the direction of the row shift, any amplitude greater than 2/ε rows can assure positive net displacement during one fluid oscillation. It is worthwhile to note that the alternating sign of the array shift angle at every vertical period of the traps was made in consideration of actual experiments (Appendix F).

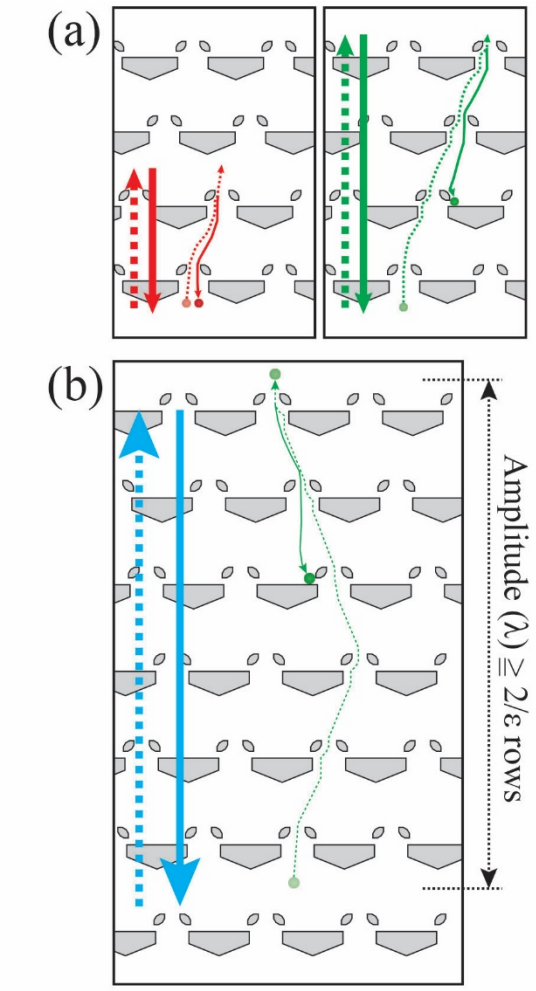

Figure 3.11: The amplitude (λ) of fluid oscillation should be greater than two vertical periods, the distance of 2/ε rows, of asymmetric traps. (a) Too small amplitude (red arrows) does not provide a chance of capture during reverse flow. On the other hand, long amplitudes (green arrows) can make positive net displacement. (b) Any amplitude greater than the distance of 2/ε rows can provide positive net displacement.

3.3.5 Experimental validation

Visual observation of trap-particle dynamics confirmed the validity of our theoretical analysis. We fabricated and tested 48 different arrays with different d^* and s^* values and with row shift fractions of 1/3 or 1/2, and most of them showed a type of trap-particle interaction predicted by our theory. One-way particle transport was observed in all of the arrays (green shaded region in Figure 3.12) that satisfied all of the critical

conditions including mechanical capture, asymmetric interaction, physical collision, and lateral shift. Also, other predicted trap-particle interactions showed good agreement with our theory: symmetric capturing interaction occurred in the region between d^*_{asymm} and d^*_{cap} as expected, and the trap skipping that causes no transport was observed in the region above d^*_{asymm} and below the area for one-way particle transport. Note that there were only a few data points (the green triangles surrounded by dashed red circles in Figure 3.12) that did not precisely fit our model, and these discrepancies were most likely due to the effect of expansion and contraction of the fluids between two trap rows on the lateral shift of the particle. Also, the variations in array fabrication and the dissimilarity between our 2D model and 3D experimental system also increase uncertainty in prediction.

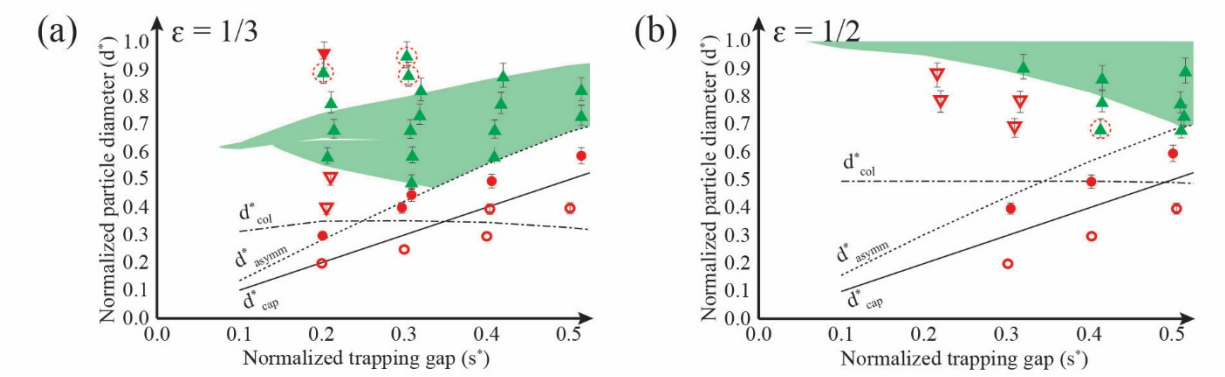

Figure 3.12: Experimental validation of the theoretical results. Theoretical prediction and experimentally validated trap-particle interaction dynamics in the arrays of row shift fraction (ε) of (a) 1/3 and (b) 1/2. A shaded region is supposed to show one-way particle transport according to the theoretical results. Each symbol of the graph (a) and (b) means types of trap-particle interaction dynamics observed in the validation experiments: green triangles (▲) for one-way particle transport, inverted closed red triangles (▼) for no-lateral displacement into the capturing stream due to steric hindrance of a large particle, inverted open triangles (▽) for no-lateral displacement into the capturing stream due to trap skipping of a small particle, closed circles (●) for symmetric capturing, and open circles (○) for symmetric passage which occurs for the particles smaller than trapping gap.

The comparison between vertical locations of particles before and after fluid oscillations clearly shows this system can transport particles arguably better than other

types of trap-particle interaction dynamics. After completion of one-way particle transport, the particles accumulate above the last rows of the array (Figure 3.13.a-3.13c). On the other hand, symmetric capturing (Figure 3.13.d) interactions had no noticeable effect, and trap skipping (Figure 3.13.e) had a slight effect on overall displacement. Slow transport was observed for the particles having steric hindrance that prevents them from entering the capturing stream (Figure 3.13.f). The mechanism of this slow displacement was different from the one-way particle transport. The path of those particles during reverse flow was longer than during forward flow, making the particles travel shorter vertical distances during reverse flow, and this difference in the vertical travel distances causes slow transport.

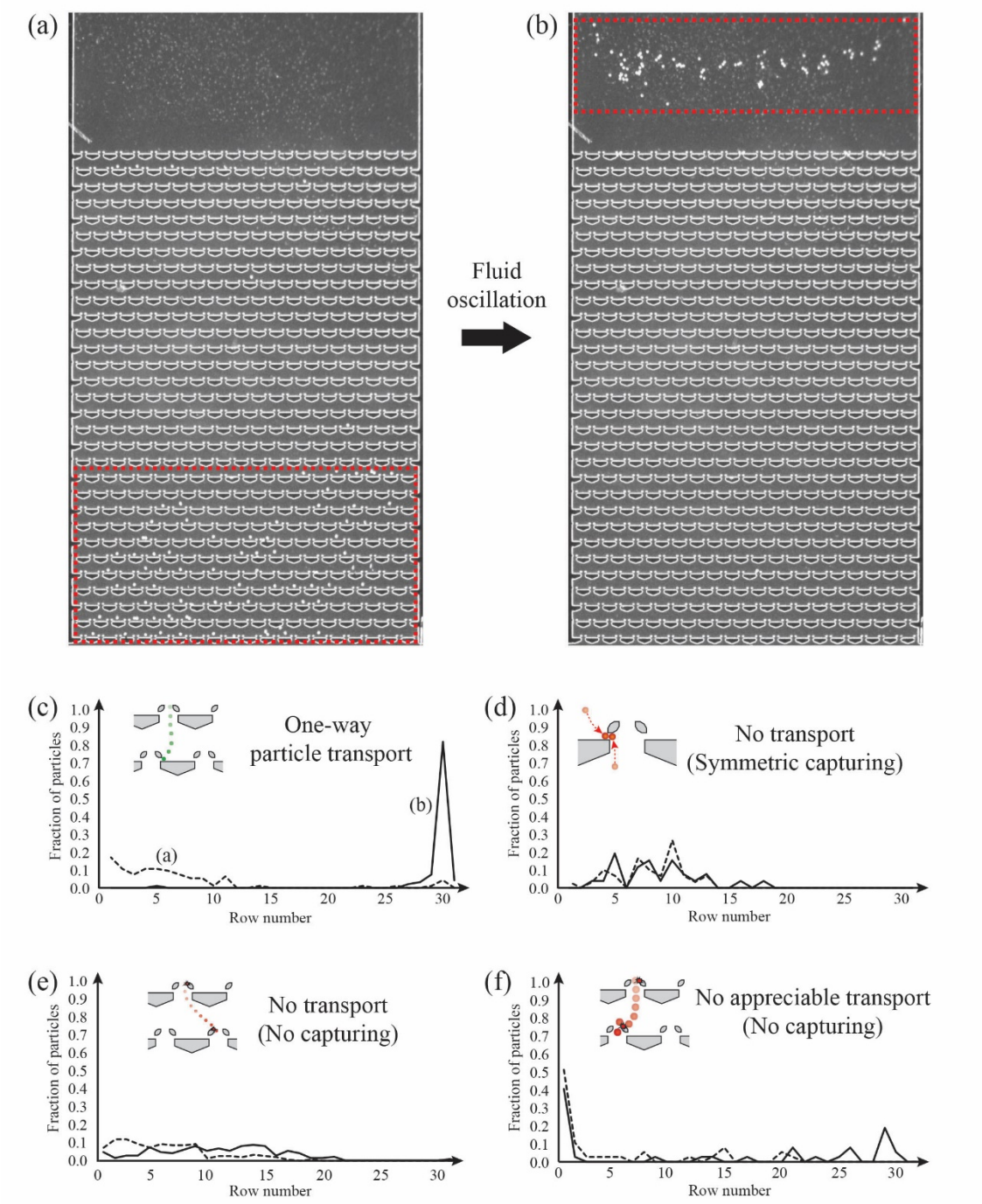

Figure 3.13: The vertical locations of the particles before and after seven fluid oscillations at various trap-particle interaction dynamics. A group of particles (surrounded by red-dashed rectangle) in the entry part of the array (a) was transported to the end region of the array (b) by one-way particle transport. (c-f) A fraction of particles at each row shows the change of particle distribution before (dashed line) and after (solid line) (c) one-way particle transport, (d) symmetric capturing, (e) no-lateral displacement into the capturing stream because of skipping traps, and (f) no-lateral displacement into the capturing stream because of large steric hindrance. The diagrams in each graph show detailed trap-particle dynamics in the reference of Figure 3.3(d) and 3.9(b).

We observed high transport ability of particles at particle concentration up to 1 % (v/v), which was equal to the average of a single particle per trap. This one-way particle transport at this high concentration could be attributed to two reasons: locally low concentration in the front line of loaded particles and the releasing of clogged particles by oscillatory flow. The particles at the front of the concentration wave always had a low concentration surrounding them, ensuring reliable transport at an overall-high concentration. As one-way particle transport continued, the concentration of the particles behind the front decreased, approaching the ideal operating conditions for one-way particle transport. Occasionally, locally high concentrations could induce clogging at inter-trapping blocks gaps, but those aggregated particles were released during fluid oscillation.

3.4 Conclusions

We have presented the theoretical foundation of one-way particle transport in oscillatory fluid flow. Passage-capture interactions between the asymmetric traps and the particles enable the positive net displacement of particles with no net displacement of fluid. Based on the understanding of the deterministic character of laminar flow through the asymmetric traps, the necessary conditions for one-way particle transport were found in terms of mechanical capture, asymmetric interaction, physical collision, and lateral shift. The critical dimensions for each condition were estimated using FEM and analytical mass balance equations. Since the analysis used in this work solely depends on the dimension of the asymmetric traps and particle diameter, the theory can be applied to any obstacle array of similar geometric configurations.

Particle dynamics in asymmetric traps can be used to serve several practical operations for manipulating micro-particles in oscillatory flow. The one-way particle transport shown in this work provides basic transport of particles with no net transport of fluid. Since the types of trap-particle interaction are a function of the particle diameters, size-based segregation can be implemented such that target particles showing one-way particle transport are isolated from other particles having non-transport trap-particle interactions such as symmetric capturing or trap skipping. Also, concentrating groups of particles is another application of this system. We believe that operations utilizing asymmetric traps will contribute to the wide use of micro-particles for the integrated microfluidic system.

3.5 References

1. L. R. Huang, E. C. Cox, R. H. Austin, and J. C. Sturm, Continuous particle separation through deterministic lateral displacement, *Science*, 2004, **304**, 987-990.

2. J. McGrath, M. Jimenez, and H. Bridle, Deterministic lateral displacement for particle separation: a review, *Lab on a Chip*, 2014, **14**, 4139-4158.

3. D. Di Carlo, Inertial microfluidics, *Lab on a Chip*, 2009, **9**, 3038-3046.

4. H. Amini, W. Lee, and D. Di Carlo, Inertial microfluidic physics, *Lab on a Chip*, 2014, **14**, 2739-2761.

5. M. Yamada, M. Nakashima, and M. Seki, Pinched flow fractionation: Continuous size separation of particles utilizing a laminar flow profile in a pinched microchannel, *Analytical Chemistry*, 2004, **76**, 5465-5471.

6. M. Yamada and M. Seki, Hydrodynamics filtration for on-chip particle concentration and classification utilizing microfluidics, *Lab on a Chip*, 2005, **5**, 1233-1239.

7. X. Xuan, J. Zhu, and C. Church, Particle focusing in microfluidic devices, *Microfluidics and Nanofluidics*, 2010, **9**, 1-16.

8. A. J. Mach, J. H. Kim, A. Arshi, S. C. Hur, and D. Di Carlo, Automated cellular sample preparation using a Centrifuge-on-a-Chip, *Lab on a Chip*, 2011, **11**, 2827-2834.

9. D. R. Gossett, W. M. Weaver, A. J. Mach, S. C. Hur, H. T. K. Tse, W. Lee, H. Amini, and D. Di Carlo, Label-free cell separation and sorting in microfluidic systems, *Analytical and Bioanalytical Chemistry,* 2010, **397**, 3249-3267.

10. C. Jin, S. M. McFaul, S. P. Duffy, X. Deng, P. Tavassoli, P. C. Black, and H. Ma, Technologies for label-free separation of circulating tumor cells: from historical foundations to recent developments, *Lab on a Chip*, 2014, **14**, 32-44.

11. Y. Chen, P. Li, P. Huang, Y. Xie, J. D. Mai, L. Wang, N. Nguyen, and T. J. Huang, Rare cell isolation and analysis in microfluidics, *Lab on a Chip*, 2014, **14**, 626-645.

12. X. Mao and T. J. Huang, Exploiting mechanical biomarkers in microfluidics, *Lab on a Chip*, 2012, **12**, 4006-4009.

13. S. M. McFaul, B. K. Lin, and H. Ma, Cell separation based on size and deformability using microfluidic funnel ratchets, *Lab on a Chip*, 2012, **12**, 2369-2376.

14. H. T. K. Tse, D. R. Gossett, Y. S. Moon, M. Masaeli, M. Sohsman, Y. Ying, K. Mislick, R. P. Adams, J. Rao, and D. Di Carlo, Quantitative diagnosis of malignant pleural effusions by single-cell mechanophenotyping, *Science Translational Medicine*, 2013, **5**, 212ra163.

15. Y. Zheng, J. Nguyen, Y. Wei, and Y. Sun, Recent advances in microluidic techniques for single-cell biophysical characterization, *Lab on a Chip*, 2013, **13**, 2464-2483.

16. R. G. Rice, Progress in parametric pumping, *Separation and Purification Methods,* 1976, **5**, 139-188.

17. R. H. Wilhelm and N. H. Sweed, Parametric pumping: Separation of mixture of Toluene and n-Heptane, *Science*, 1968, **159**, 522-524.

18. R. H. Wilhelm, A. W. Rice, R. W. Rolke, and N. H. Sweed, Parametric pumping. A dynamic principle for separating fluid mixtures, *Industrial & Engineering Chemistry Fundamentals*, 1968, **7**, 337-349.

19. K. Liu, R. Wu, Y. Chuang, H. S. Khoo, S. Huang, and F. Tseng, Microfluidic systems for biosensing, *Sensors*, 2010, **10**, 6623-6661.

20. A. van Reenen, A. M. de Jong, J. M. J. den Toonder, and M. W. J. Prins, Integrated lab-on-chip biosensing systems based on magnetic particle actuation - a comprehensive review, *Lab on a Chip*, 2014, **14**, 1966-1986.

21. J. Choi, K. W. Oh, J. H. Thomas, W. R. Heineman, H. B. Halsall, J. H. Nevin, A. J. Helmicki, H. T. Henderson, and C. H. Ahn, An integrated microfluidic biochemical detection system for protein analysis with magnetic bead-based sampling capabilities, *Lab on a Chip*, 2002, **2**, 27-30.

22. C. -H. Chiou, D. J. Shin, Y. Zhang, T. -H. Wang, Topography-assisted electromagnetic platform for blood-to-PCR in a droplet, *Biosensors and Bioelectronics*, 2013, **50**, 91-99.

23. N. Beyor, L. Yi, T. S. Seo, and R. A. Mathies, Integrated capture, concentration, polymerase chain reaction, and capillary electrophoretic analysis of pathogens on a chip, *Analytical Chemistry*, 2009, **81**, 3523-3528.

24. C. -H. Wang, K. -Y. Lien, T. -Y. Wang, T. -Y. Chen, and G. -B. Lee, An integrated microfluidic loop-mediated-isothermal-amplification system for rapid sample pre-

treatment and detection of viruses, *Biosensors and Bioelectronics*, 2011, **26**, 2045-2052.

25. T. Maleki, T. Fricke, J. T. Quensenberry, P. W. Todd, and J. F. Leary, Point-of-care, portable microfluidic blood analyzer system, *Proceedings SPIE 8251,* 2012, DOI: 10.1117/12.909051.

26. L. Cui, T. Zhang, and H. Morgan, Optical particle detection integrated in a dielectrophoretic lab-on-a-chip, *Journal of Micromechanics and Microengineering*, 2002, **12**, 7-12.

27. J. D. Yantzi, J. T. W. Yeow, and S. S. Abdallah, Multiphase electrodes for microbead control applications: Integrateion of DEP and electrokinetics for bio-particle positioning, *Biosensors and Bioelectronics*, 2006, **22**, 2539-2545.

28. J. Ramón-Azcón, T. Yasukawa, and F. Mizutani, Sensitive and spatially multiplexed detection system based on dielectrophoretic manipulation of DNA-encoded particles used a immunoreactions platform, *Analytical Chemistry*, 2011, **83**, 1053-1060.

29. J. Ramón-Azcón, T. Yasukawa, and F. Mizutani, Immunodevice or simultaneous detection of two relevant tumor markers based on separation of different microparticles by dielectrophoresis, *Biosensors and Bioelectronics*, 2011, **28**, 443-449.

30. J. Ramón-Azcón, T. Yasukawa, H. J. Lee, T. Matsue, F. Sánchez-Baeza, M. -P. Marco, and F. Mizutani, Competitive multi-immunosensing of pesticides based on the particle manipulation with negative dielectrophoresis, *Biosensors and Bioelectronics*, 2010, **25**, 1928-1933.

31. Z. Zou, S. Lee, and C. H. Ahn, A polymer microfluidic chip with intedigitated electrodes arrays for simultaneous dielectrophoretic manipulation and impedimetric detection of microparticles, *IEEE Sensors Journal*, 2008, **8**, 527-535.

32. B. Çetin and D. Li, Dielectrophoresis in microfluidics technology, *Electrophoresis*, 2011, **32**, 2410-2427.

33. P. Glynne-Jones, R. J. Boltryk, M. Hill, F. Zhang, L. Dong, J. S. Wilkinson, T. Melvin, N. R. Harris, and T. Brown, Flexible acoustic particle manipulation device with integrated optical waveguide for enhanced microbead assays, *Analytical Sciences*, 2009, **25**, 285-291.

34. T. Lilliehorn, M. Nilsson, U. Simu, S. Johansson,, M. Almqvist, J. Nilsson, T. Laurell, Dynamic arraying of microbeads for bioassays in microfluidic channels, *Sensors and Actuators B*, 2005, **106**, 851-858.

35. S. -C. S. Lin, X. Mao, and T. J. Huang, Surface acoustic wave (SAW) acoustophoresis: now and beyond, *Lab on a Chip*, 2012, **12**, 2766-2770.

36. L. Y. Yeo and J. R. Friend, Surface acoustic wave microfluidics, *Annual Review of Fluid Mechanics*, 2014, **46**, 379-406.

37. M. Manesse, A. F. Phillips, C. N. LaFratta, M. A. Palacios, R. B. Hayman, and D. R. Walt, Dynamic microbead arrays for biosensing applications, *Lab on a Chip*, 2013, **13**, 2153-2160.

38. H. C. Hunt and J. S. Wilkinson, Optofluidic integration for microanalysis, *Microfluidics and Nanofluidics,* 2008, **4**, 53-79.

39. J. Lee and M. A. Burns, Asymmetric traps array for particle transport, *RSC Advances*, 2015, **5**, 3358-3364.

40. K. Loutherback, J. Puchalla, R. H. Austin, and J. C. Sturm, Deterministic microfluidic ratchet, *Physical Review Letters*, 2009, **102**, 045301.

41. D. W. Inglis, J. A. Davis, R. H. Austin, and J. C. Sturm, Critical particle size for fractionation by deterministic lateral displacement, *Lab on a Chip*, 2006, **6**, 655-658.

Chapter IV

PARTICLE OPERATIONS USING ASYMMETRIC TRAPS

4.1 Introduction

Operations of micro-particles suspended in fluids are essential for current life science and medical diagnostics. The micro-particles covered with molecular probes are very popular tool for quantifying bio-chemicals via nucleic acids hybridization [1, 2] or protein immuno-precipitation. [3-5] With those micro-particles, the flow cytometers have greatly reduced the time and cost for chemical analysis via reading of the signals from multiplexed microbeads in extreme high-throughput. Also, encoded microbeads placed on two dimensional array of microwells are being used for the highly multiplexed analysis of nucleic acids. The use of micro-particles is not limited to bench-top instruments. Many portable health care devices use magnetic microbeads for facile isolation of biomarkers from specimen. [9,10] The technologies used for the operation of micro-particles can also be utilized for the manipulation of cells.

Deterministic dynamics of fluids and particles in low Reynolds number of microfluidics have led to the development of microfluidic passive techniques for micro-particle operations. Deterministic lateral displacement capitalizes on characteristic flow field shaped by periodic obstacle array, which induces predictable lateral shift of micro-particles in the array. [11-13]

Inertial microfluidics uses a balance between inertial lift forces applied to micro-particles confined in a microfluidic channel, resulting in locating the particles in equilibrium position of cross-section or uniform spacing between micro-particles. [14-16] Other passive fluidic techniques [17, 18] including the pinched flow fractionation, [19,20] hydrophoresis, [21,22] and microparticle railing [23,24] use characteristic flow field formed by geometry of the microchannel. These microfluidic passive techniques have shown promising results in various applications such as separation of cells by their size or deformability and chemical treatment of cells.

While most of the microfluidic passive techniques rely on continuous flow, the use of oscillatory flow, a time-dependent alternating flow field, can extend the applicability of the micro-particles. Since it has no net displacement of fluid, it can be implemented in a closed fluidic circuit, which is advantageous for integration in Lab-on-a-Chip devices for multi-step process. Also, it can minimize the footprint necessary for fluid handling, which is critical for mobile point-of-care devices. In the Chapter 2, we introduced the asymmetric trap, a physical trap that has unique trap-particle interactions, for transport of micro-particles in oscillatory flow. [25] In the Chapter 3, the asymmetric traps could displace micro-particles with negligible overall net displacement of fluid, which showed possibility of particle operations in oscillatory flow.

In this chapter, as a proof of concept, we demonstrate micro-particle operations in oscillatory flow by using the asymmetric traps. The characteristic physical interactions with micro-particles and transport polarity of the asymmetric traps enabled segregation, medium exchange, and focusing and splitting of micro-particles in oscillatory flow. The different transport speeds of the size-dependent trap-particle interactions could lead to the segregation of a mixture of micro-particles. The asymmetric traps could displace the particles from one medium

to the other medium more quickly than the advance of mixing front, which resulted in medium exchange of the micro-particles in oscillatory flow. Transport polarity of the asymmetric traps enabled multiple arrays of the traps to focus or split groups of micro-particles in specific designated areas. We believe that these functions using asymmetric traps would promote the use of micro-particles for various circumstances including portable and integrated multi-step reaction devices.

4.2 Materials and methods

4.2.1 Fabrication of the microfluidic device

Microfluidic devices consist of three layers including fluidic channel made of Si, control channel made of polydimethylsiloxane (PDMS), and thin PDMS membrane separating two channels. The geometry of the device was shown in our previous work. Only the dimension of the asymmetric traps of the devices were modified for each condition of the most experiment, but the focusing and splitting experiments used the devices with a modified geometry to change the loading region of the particles. The Si structure of the fluidic channel was shaped via photolithography and dry etching. A photoresist (SPR 955CM, Microchem Corp.) was coated at 3000 rpm on a Si wafer, and exposed by a mask aligner (MA/BA6 mask aligner, Karl Suss MicroTec) for 5 sec after a pre-bake for 1 min at 100 ^{o}C on a hot plate. The exposed resist was developed (AZ$^{®}$726, MicroChemicals) after a post-bake for 1 min at 110 ^{o}C on a hot plate. Deep reactive ion etching (DRIE) (STS Pegasus 4, SPTS Technologies, Ltd.) was applied to the exposed area so that a fluidic channel was built on the Si surface. The height of the channel was about 40 μm. Control channel of PDMS was cast on the mold made of Si. The pattern on the mold was shaped by photolithography and DRIE as done for the Si fluidic channel. Then, the

surface of the mold was passivated by a trichlorosilane ((tridecafluoro-1,1,2,2-tetrahydrooctyl)-1-trichlorosilane, UCT) via chemical vapor deposition on plasma-activated surface. The PDMS monomer and cross-linker were mixed (10:1 w/w ratio) and poured in the mold. The PDMS and mold was heated at 80 ^{o}C for 1.5 hr in an oven after degassing. The height of the control channel was about 100 μm. The thin PDMS membrane was spin-coated and cured on a Si wafer. The PDMS mixture (10:1 monomer:cross-linker w/w ratio) was spin-coated at 600 rpm and cured at 140 ^{o}C for 3 hrs on a hot plate. After finishing the fabrication of each part, those are aligned and attached via plasma bonding. The locations where normally-closed valves are placed are masked with PDMS pieces to block bonding.

4.2.2 Implementation of fluidic system

LabView application was used to control the valve operation and fluid oscillation. The inlets of the control channel were connected to the pneumatic pressure sources. The LabView-controlled regulators and solenoid valves adjusted the pressure, and the number and amplitude of fluid oscillations, respectively. The amplitude of the fluid oscillation was controlled via adjustment of the duration of solenoid valve opening.

4.2.3 Preparation of micro-particle solutions

Binary mixture of the particles of 30.2 μm and 20.4 μm diameter were used for the segregation. The particles were re-suspended in the density-equilibrated buffer that is a mixed solution of deionized water, OptiPrep^{TM} density gradient medium (Sigma-Aldrich Co.), and Tween 20 surfactant of 0.1 % v/v (Sigma-Aldrich Co.). The number of the particles in the array was adjusted by varying the concentration of the particles. For multiplexed segregation, the

particles of 10.1, 20.4, and 30.2 μm diameter were used. The experiments of the focusing and splitting used a solution of 30.2 μm particle.

The experiments of medium exchange used two solutions including the density-equilibrated buffer and a Fluorescein solution (0.004 g/mL of Fluorescein Sodium salt dissolved in the density equilibrated buffer) (Sigma-Aldrich, Co.). Before the experiment, the particle of 30.2 μm diameter was re-suspended in the Fluorescein solution. Once the fluorescein solution was loaded into the device filled with the density-equilibrated buffer, the oscillatory flow the particles were displaced from the fluorescein solution to the buffer. The fluorescence of the array region was measured before and after the segregation.

4.2.4 Image analysis

The images of the fluorescence of particles and fluids were taken by a ccd camera (Grasshopper®3, Point Grey Research, Inc.) mounted on the top of a stereo microscope (SZX12, Olympus Corp.). Both white light and fluorescence images were taken on the regions of the asymmetric traps both before and after the fluid oscillations (Image J. v.1.49). Then, row number marks in the white light image were copied and pasted at the same area of the fluorescence image. Then, the number of particles at each row was counted. In the data analysis for medium exchange experiment, the location of mixing front was decided as a maximum row number that has fluorescence intensity higher than the sum of average and two standard deviation of fluorescence intensity of non-fluorescent buffer region in the image captured before fluid oscillation.

4.3 Results and discussion

4.3.1 Concept of micro-particle operations using asymmetric traps

Asymmetric traps provide flexible operations of micro-particles based on two unique features including characteristic size-dependent trap-particle interactions and transport polarity of asymmetric traps. First, the types of trap-particle interactions are varied by the diameter of the particles at a given dimension of asymmetric traps, and those interactions have different transport speed of the particles in oscillatory flow (Figure 4.1.a). Second, in the regime of one-way particle transport, one of the trap-particle interactions, the asymmetric traps have transport polarity: they play as a role of either blocker or open-channel depending on the direction of the particle movement in the asymmetric traps (Figure 4.1.b). These elements of array design are independent of each other, providing flexibility to the application of the asymmetric traps.

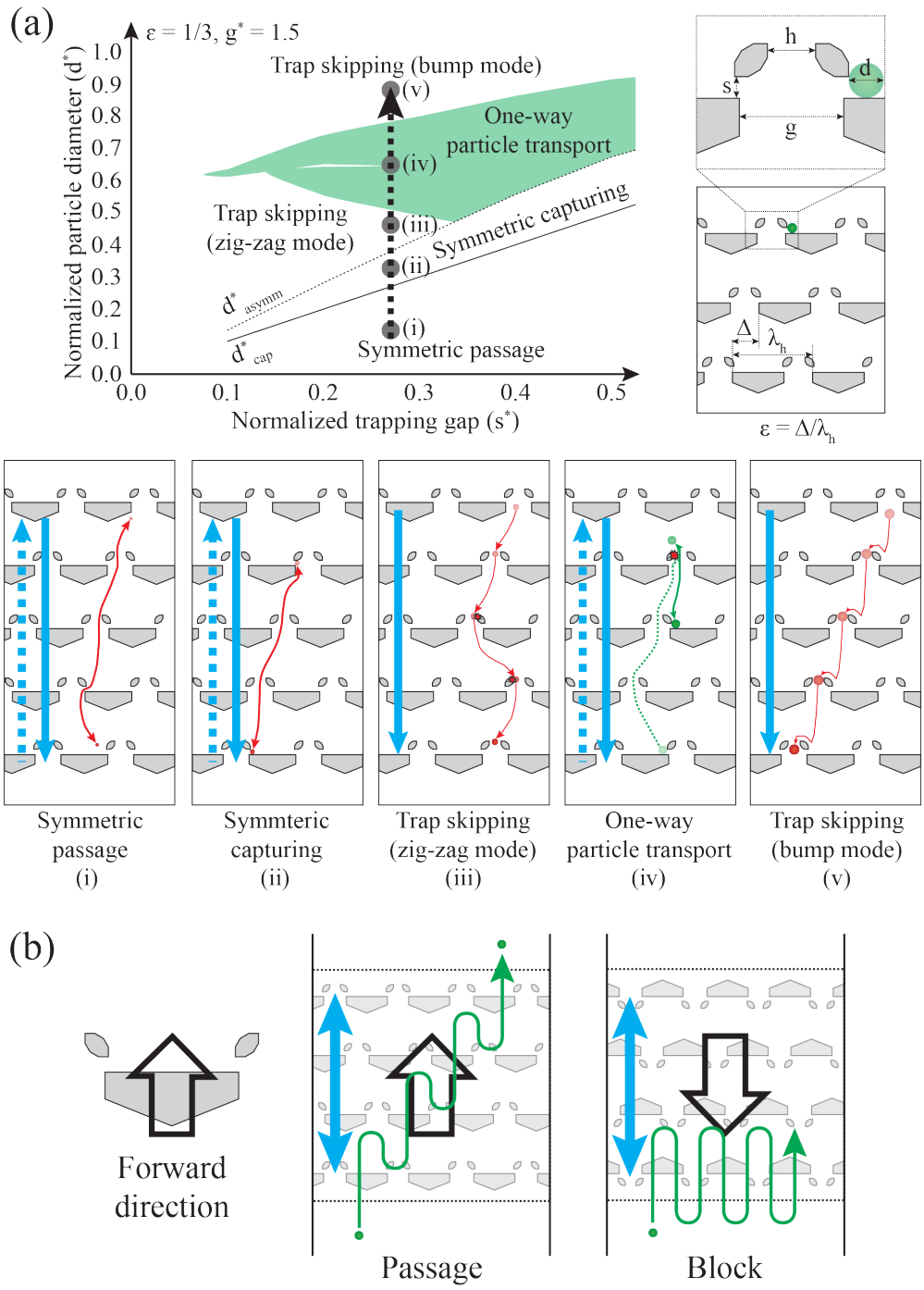

Figure 4.1: Two unique features of asymmetric traps. (a) Five types of trap-particle interactions. As the diameter of a particle increases at a given dimension of the array, the trap-particle interaction changes. (b) Transport polarity of asymmetric traps. In the regime of one-way particle transport, the particles can only be transported along forward direction of the array. Therefore, the array either allows the passage of the particles or blocks the particles depending on relative location of the particles to the array. The superscript "*" means the normalization by inter-trapping blocks gap, h. It should be noted that lateral displacement of the arrow in (b) is only for clear description of vertical motion of the particles. The particles show only vertical movement.

The difference in transport speeds of size-dependent trap-particle interactions enables spatial separation of micro-particles based on their diameters (Figure 4.2.a). In the Chapter 3, we found that the one-way particle transport has superb transport speed among five different types of trap-particle interactions. With a few fluid oscillations, one-way particle transport displaced micro-particles across tens of rows while other trap-particle interactions showed no appreciable transport. This distinct difference in transport ability of the trap-particle interactions allows the particles having the one-way particle transport to be isolated from the particles of the other regimes of the trap-particle interactions.

The transport polarity of the asymmetric traps enables multiple arrays of different directions to serve functions such as focusing or splitting in oscillatory flow. Since transport polarity of the asymmetric traps determines the direction of particle transport, careful design of the directions of multiple arrays can displace a group of particles to a number of locations at a single operation. For example, two arrays heading toward each other can focus micro-particles that initially stayed outside of the arrays into the central area (Figure 4.2.b). On the other hand, the arrays heading away from each other can split a group of micro-particles at a number of separate areas. Groups of particles can be distributed to or gathered at almost limitless number of spots very efficiently via just a few fluid oscillations.

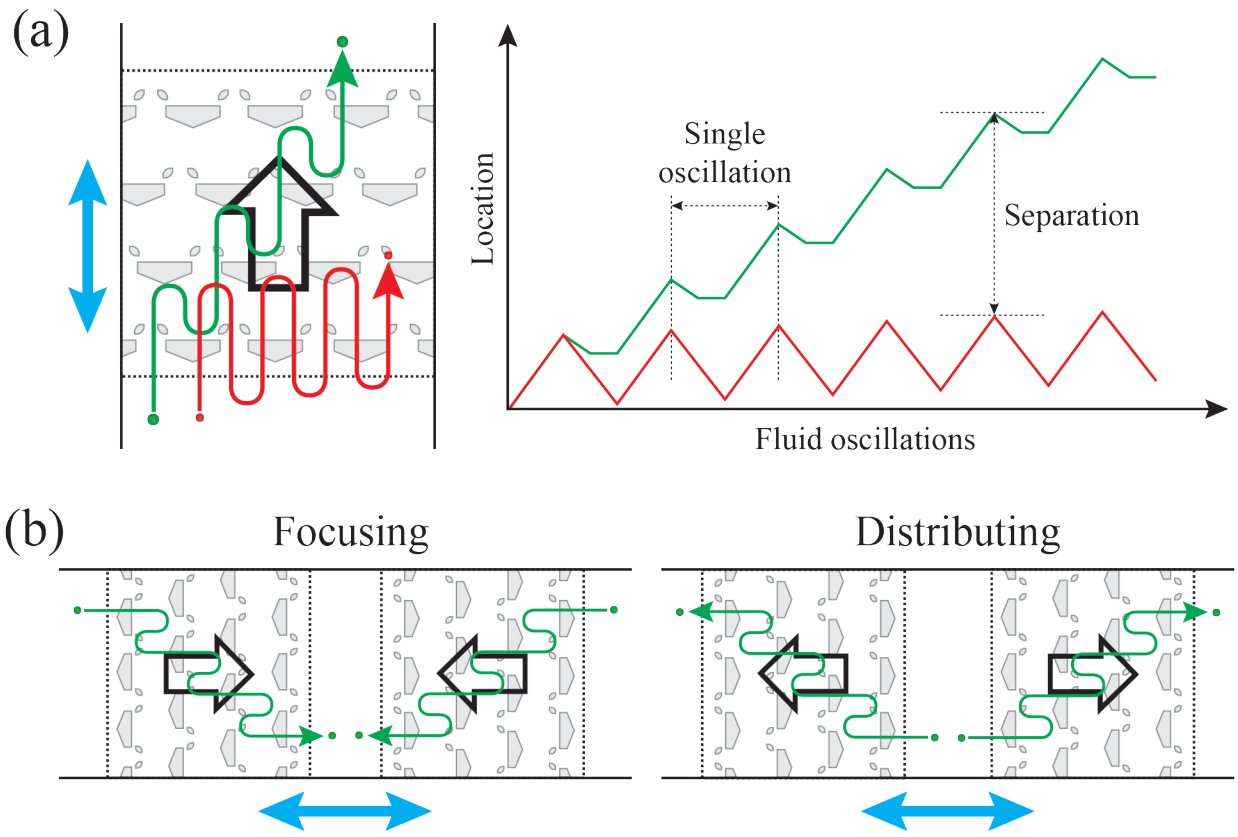

Figure 4.2: Example of utilizing the features for particle operation. (a) Size-based particle separation. The speed of one-way particle transport is much faster than it of the other interactions. As fluid oscillations proceeds, the spatial separation between target (green) and non-target (red) particles increases. (b) Particle focusing and distributing with multiple arrays having opposite direction. The arrays heading towards can focus the particles at the central area of the arrays. On the other hand, the arrays heading away each other can allocate the particles into desired regions. It should be noted that lateral displacement of the arrows is only for clear description of vertical motion of the particles. The particles move along only vertical direction of the array.

4.3.2 Segregation of micro-particles

We conducted the segregation of the micro-particles in the regime of one-way particle transport from the particles of the symmetric capturing interaction. Compared to the target particles that show displacement across multiple rows at each fluid oscillation, the non-target particles of the symmetric capturing are hard to advance through the array due to trapping during forward movement (Figure 4.3). Therefore, the target particle of one-way particle transport can be isolated at the end region of the array from the mixture of the particles. The graph of interaction regimes obtained from the Chapter 3 allows users to easily determine the dimension

of the array for the particle segregation (Appendix A). The interaction regimes that can implement this segregation are not limited to one-way particle transport and symmetric capturing. Other combinations of interaction regimes such as one-way particle transport vs. symmetric passage or trap skipping can be used for segregation.

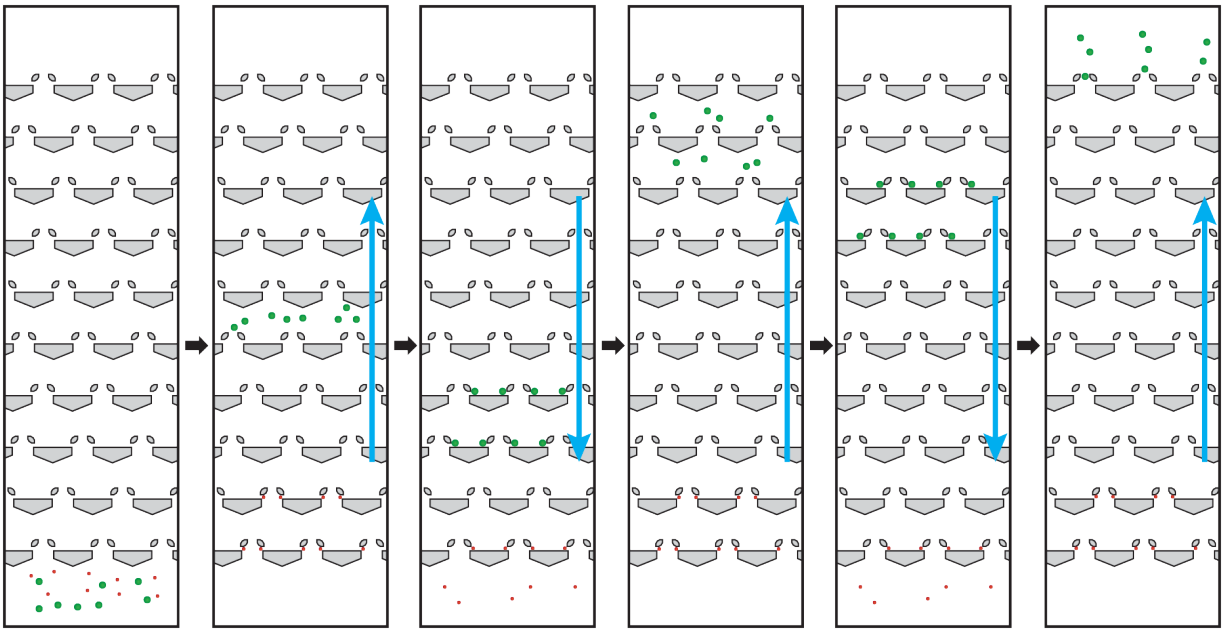

Figure 4.3: Segregation of target particles (green) exhibiting one-way particle transport from non-target particles (red) in symmetric capturing regime.

To assess the performance of the segregation, we defined three performance factors including the degree of segregation, yield, and purity of the segregation product. The definition of each factor is shown below.

$$\text{Degree of segregation} = \frac{N_{ntp}|_{ntp} + N_{tp}|_{tp}}{N_p} \tag{1}$$

$$\text{Yield} = \frac{N_{tp}|_{tp}}{N_{tp}} \tag{2}$$

$$\text{Purity} = \frac{N_{tp}|_{tp}}{N_p|_{tp}} \tag{3}$$

where N_{tp} is the number of target particles, N_{ntp} is the number of non-target particles, N_p is the total number of particles, respectively. It should be noted that the vertical bar and subscript behind it means target particle-side or non-target particle-side of distinctly separated two groups of segregation product.

Investigation of the effect of the array capacity on the segregation revealed that a number of trap row is a critical factor for high performances of the segregation at a given number of particles (Figure 4.4). To quantify the capacity of asymmetric traps, we introduced a concept of bandwidth, a number of trap rows where the particles are scattered after fluid oscillations (Appendix G). We experimentally measured the bandwidth of both target and non-target particles, and found that the bandwidth of target particles is linearly proportional to the total number of it while the bandwidth of non-target particles is scaled with a square root of total number of non-target particles (Appendix G). The segregation performances reached to its maximum value, as the ratio of the number of trap rows to the bandwidth of total particles became unity.

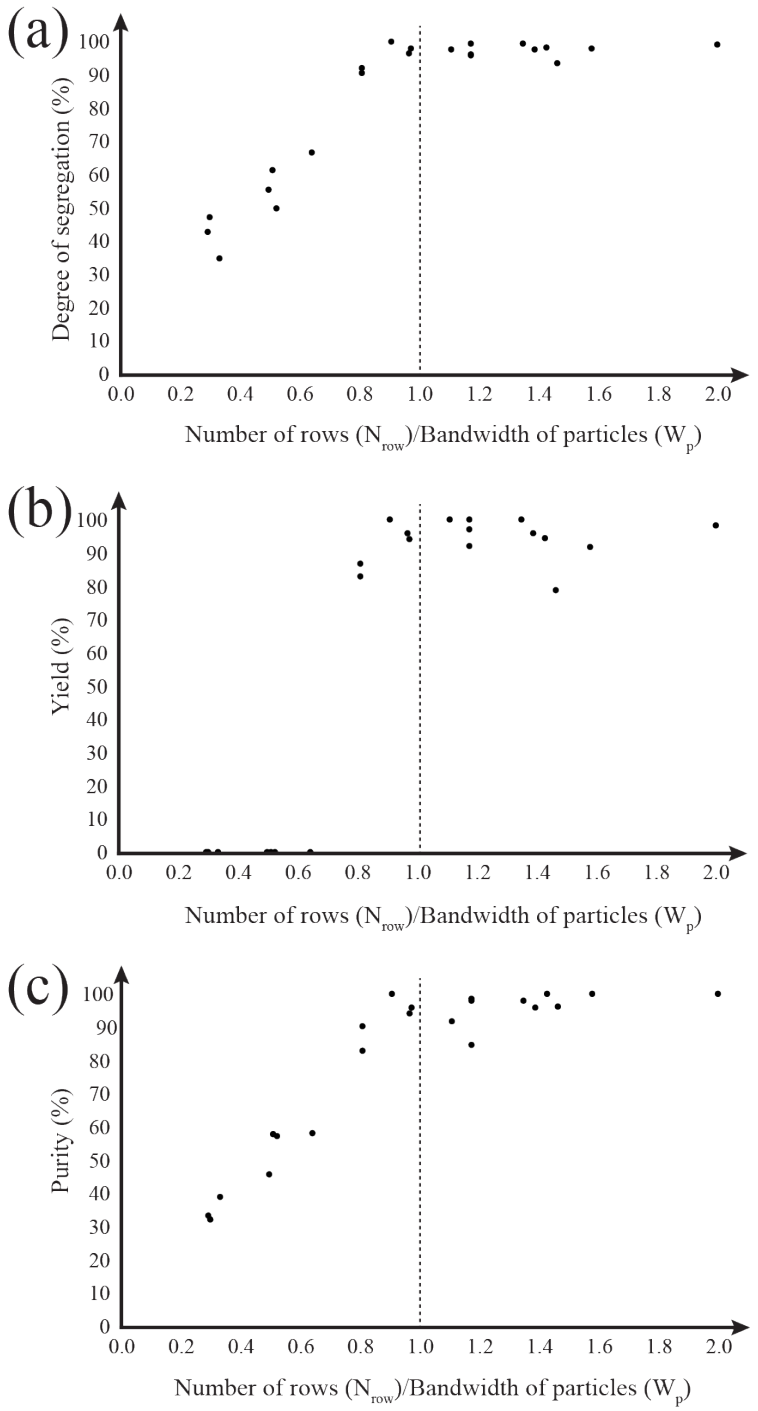

Figure 4.4: The segregation performances as a function of the ratio of number of trap rows (N_{row}) to the bandwidth of total particles (W_p). All of the segregation performances including (a) the degree of segregation, (b) yield, and (c) purity of the segregation reached high values (>90%) as the ratio of the N_{rows} to the W_p became 1.0.

The amplitude of fluid oscillation was found to be relevant with the speed of segregation, but not with the segregation performances in the tested range (Figure 4.5). As the amplitude of

fluid oscillation increased, the time to reach to high value of segregation performance factors decreased. Regardless of the amplitudes, high degree of segregation and yield of the segregation were achieved.

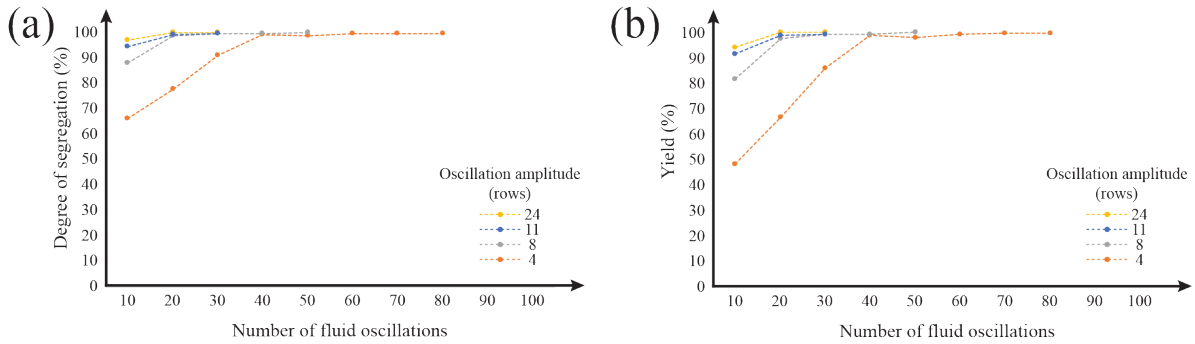

Figure 4.5: The segregation performances as a function of number of fluid oscillations at various amplitudes of fluid oscillation. The number of rows was 60. Both of the performance factors reached to high value (>99%) after numbers of fluid oscillation regardless of the amplitudes. (a) The degree of segregation as a function of the number of the fluid oscillations. As the amplitude of the oscillation increased, high degree of segregation was more quickly achieved. (b) The yield of the segregation as a function of the number of fluid oscillations. The oscillation number for high yield of the segregation was smaller for larger amplitude of oscillation.

Multiplexed segregation using multiple arrays in series was successfully implemented. The first array selectively transported large and medium sized micro-particles of ternary mixture, and following second array only transport the large particle of the segregation product of the first array (Figu43 4.6.a). The efficiency (~95%) was slightly lower than the result (>99%) of segregation of binary mixture described above (Figure 4.5.b). This can be attributed to the interaction regime of non-target particles used for the multiplexed segregation. They have symmetric passage interaction that does not block the particles in forward flow so that a part of the non-target particles advance across the array further than the particles of symmetric capturing.

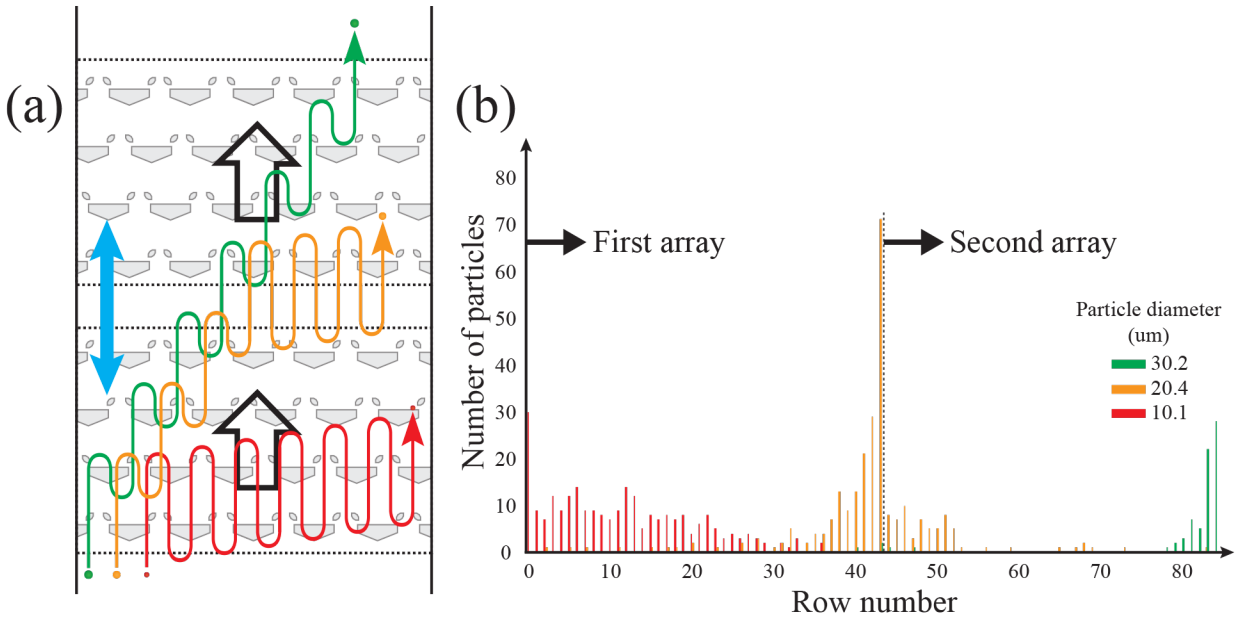

Figure 4.6: Multiplexed segregation using two arrays in series. (a) The first array transport large (green) and medium-sized (yellow) particles. Among those two particles, only large particle is transported by the second array. The small (red) particles stays in the region of the first array. (b) The distribution of the particles after segregation. It should be noted that lateral displacement of the arrows is only for clear description of vertical motion of the particles. The particles move along only vertical direction of the array.

4.3.3 Medium exchange of micro-particles

Medium exchange of micro-particles can be implemented by displacing micro-particles from one medium to the other medium during fluids oscillation across the asymmetric traps (Figure 4.7). In the oscillation of initially non-mixed two fluids in a closed chamber, the one-way particle transport of the particles and mixing of the fluids occurs simultaneously. If the speed of the particle transport is faster than the propagation of mixing front, the initial surrounding medium of a micro-particle is replaced with a new medium. Otherwise, the particles will still be under the effect of the initial medium.

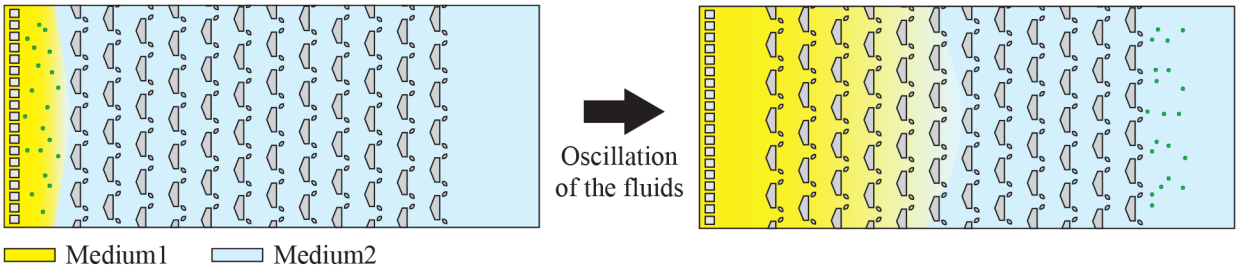

Figure 4.7: Schematic of medium exchange of micro-particles using asymmetric traps. The particles were moved from the medium 1 to the medium 2. The medium exchange can occur when the speed of one-way particle transport is faster than the speed of propagation of mixing front.

We found that modest amplitude and number of fluid oscillation are conducive to achieve clear medium exchange (Figure 4.8). Convective mixing is enhanced as amplitude of fluid oscillation increases, while small amplitude may not provide the transport speed enough for the medium exchange. Greater numbers of fluid oscillation increases processing time, which leads to high mixing ratio by diffusion. The moving speed of mixing front can vary by factors such as concentration of mediums, dimension and density of the asymmetric traps, and Reynolds number of oscillatory flow. It should be noted that faster isolation of micro-particles after medium exchange is significant because diffusion keeps occurring for prolonged waiting time.

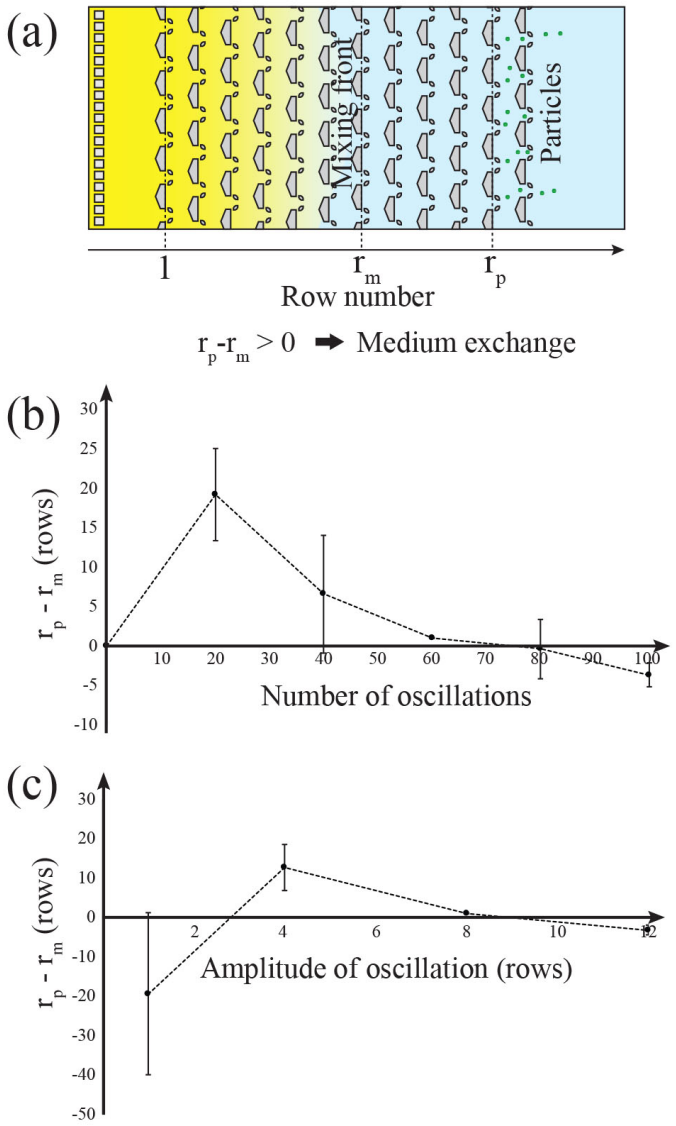

Figure 4.8: The effect of the amplitude and number of fluid oscillation on medium exchange. (a) Judgment of the medium exchange. When the last particle is in front of the mixing front (r_p-r_m > 0) after the fluid oscillations, we consider the medium exchange of the particles occurred. (b) The results of medium exchange at various numbers of fluid oscillations. (c) The results of medium exchange at various oscillation amplitudes.

4.3.4 Focusing and splitting of micro-particles

Multiple arrays facing towards each other can focus micro-particles at the central area of the arrays (Figure 4.9.a). Once the particles enter the region of two arrays heading towards each other, the particles are forced to move to the central area of the arrays due to the transport polarity of asymmetric traps. One advantage of this particle focusing is that focusing at multiple

spots is readily achievable by a single operation. Also, it can be implemented in the presence of non-target particles in the trap-particle interaction regimes such as symmetric passage. The operation capitalizing on the transport polarity of the asymmetric traps is not limited to the particle focusing. Reversing the directions of the arrays can change the operation from focusing to splitting.

The particles initially distributed across a fluidic chamber were successfully focused on the area between two arrays after fluid oscillations (Figure 4.9.b). As long as the particles could be introduced in the array region, the particles were displaced into the central region. It is worthwhile to note that the number of the particles that the array can focus is equivalent to the capacity of the arrays. The particles not focused in the array region are left outside of the array. This leaky-character of the particle focusing can be utilized for sampling of the process.

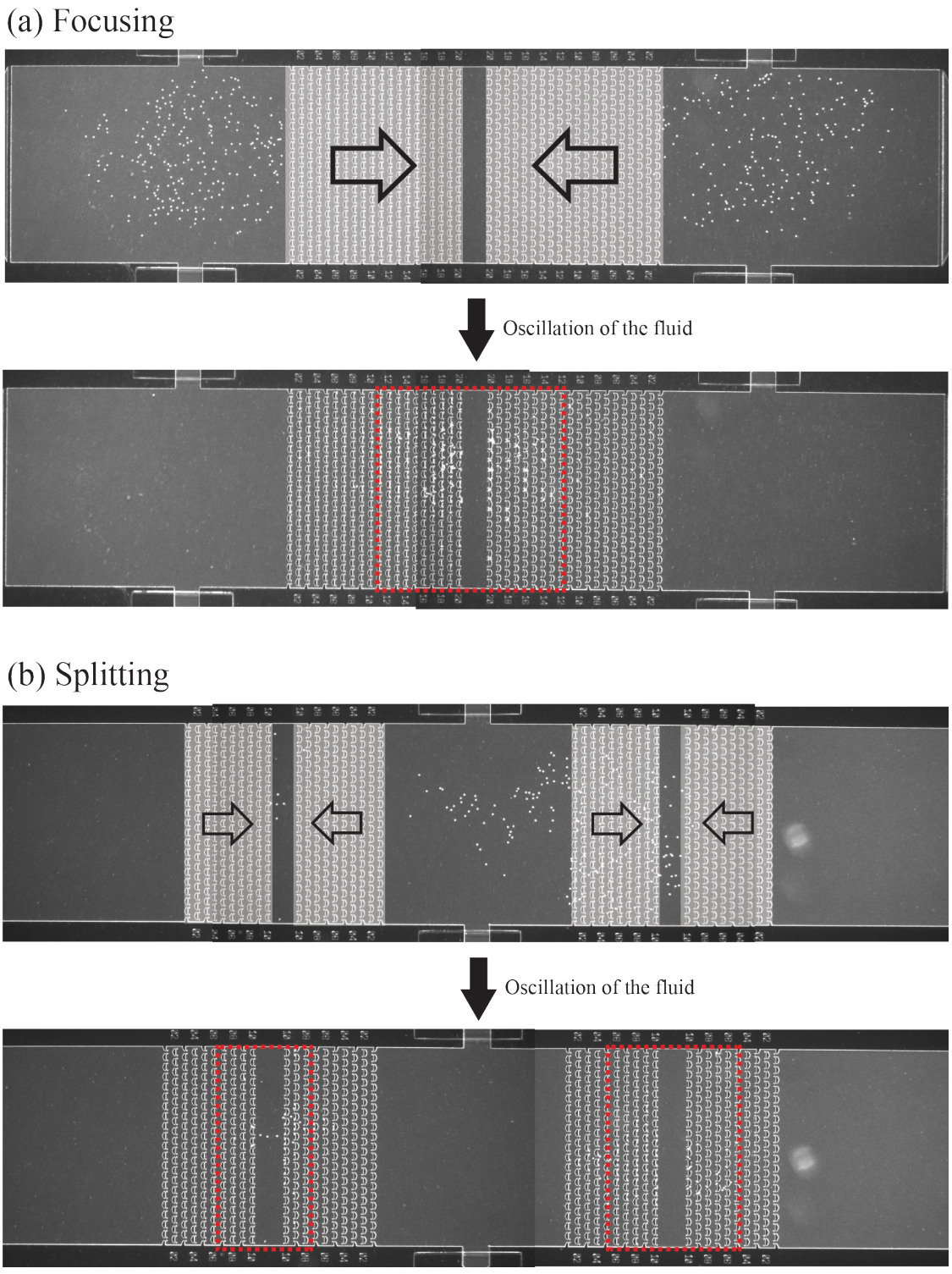

Figure 4.9: Particle (a) focusing and (b) splitting using asymmetric traps. Groups of particles are focused or splitted into the area surrounded red dashed boxes after fluid oscillations.

4.4 Conclusions

In this article, we demonstrated three example operations using asymmetric traps. Particle segregation could isolate target particles by one-way particle transport from the non-target particles that has symmetric capturing interaction with asymmetric traps. Mediums around the particles were exchanged by displacing the particles from one medium to the other in the ahead of the mixing front of the fluids. Using transport polarity of the asymmetric traps, the particles were focused on the central area of two arrays heading towards each other. These operations can be multiplexed or have new functionality by adjusting the types of trap-particle interactions, transport polarity, and varying number of arrays.

Among many possible application areas, miniaturized point-of-care device is particularly interesting application due to several characteristics of this technology. At first, the oscillatory flow can be readily made by mechanical actuation that includes manual operation. The performances of these operations were robust in a range of fluids velocity scales from μm/s to cm/s (data not shown), which promises stable performance in manual pumping operation. Also, it can process hundreds of the particles in a very short time period (<1 min), which is great advantage for the point-of-care devices whose work is time-sensitive. Therefore, we look forward to the contribution of this technology to solving global health problems.

4.5 References

1. Y. Li, Y. T. H. Cu, and D. Luo, Multiplexed detection of pathogen DNA with DNA-based fluorescence nanobarcodes, *Nature Biotechnology*, 2005, **23**, 885-889.

2. A. Spiro, M. Lowe, and D. Brown, A bead-based method for multiplexed identification and quantitation of DNA sequences using flow cytometry, *Applied and Environmental Microbiology*, 2000, **66**, 4258-4265.

3. K. L. Kellar, R. R. Kalwar, K. A. Dubois, D. Crouse, W. D. Chafin, and B.-E. Kane, Multiplexed fluorescent bead-based immunoassays for quantitation of human cytokines in serum and culture supernatants, *Cytometry Part A*, 2001, **45**, 27-36.

4. M. E. Arellano-Garcia, S. Hu, J. Wang, B. Henson, H. Zhou, D. Chia, and D. T. Wong, Multiplexed immunobead-based assays for detection of oral cancer protein biomarkers in saliva, *Oral Diseases*, 2008, **14**, 705-712.

5. D. A. A. Vignali, Multiplexed particle-based flow cytometric assays, *Journal of Immunological Methods*, 2000, **243**, 243-255.

6. K. L. Kellar and M. A. Iannone, Multiplexed microsphere-based flow cytometric assays, *Experimental Hematology*, 2002, **30**, 1227-1237.

7. S. A. Dunbar, Applications of Luminex® xMAP™ technology for rapid high-throughput multiplexed nucleic acid detection, *Clinica Chimica Acta*, 2006, **363**, 71-82.

8. J.-B. Fan, K. L. Gunderson, M. Bibikova, J. M. Yeakley, J. Chen, E. W. Garcia, L. L. Lebruska, M. Laurent, R. Shen, and D. Barker, [3] Illumina universal bead arrays, *Methods in Enzymology*, 2006, **410**, 57-73.

9. J. J. Chalmers, M. Zborowski, L. Sun, and L. Moore, Flow through, immunomagnetic cell separation, *Biotechnology Progress*, 1998, **14**, 141-148.

10. C.-H. Wang, K.-Y. Lien, T.-Y. Wang, T.-Y. Chen, and G.-B. Lee, An integrated microfluidic loop-mediated-isothermal-amplification system for rapid sample pre-treatment and detection of viruses, *Biosensors and Bioelectronics*, 2011, **26**, 2045-2052.

11. L. R. Huang, E. C. Cox, R. H. Austin, and J. C. Sturm, Continuous particle separation through deterministic lateral displacement, *Science*, 2004, **304**, 987-990.

12. D. W. Inglis, J. A. Davis, R. H. Austin, and J. C. Sturm, Critical particle size for fractionation by deterministic lateral displacement, *Lab on a Chip*, 2006, **6**, 655-658.

13. K. J. Morton, K. Loutherback, D. W. Inglis, O. K. Tsui, J. C. Sturm, S. Y. Chou, and R. H. Austin, Hydrodynamic metamaterials: Microfabricated arrays to steer, refract, and focus

streams of biomaterials, *Proceedings of National Academy of Sciences of the United States of America*, 2008, **105**, 7434-7438.

14. D. Di Carlo, Inertial microfluidics, *Lab on a Chip*, 2009, **9**, 3038-3046.

15. H. Amini, W. Lee, and D. Di Carlo, Inertial microfluidic physics, *Lab on a Chip*, 2014, **14**, 2739-2761.

16. J. Zhang, S. Yan, D. Yuan, G. Alici, N.-T. Nguyen, M. E. Warkiani, and W. Li, Fundamentals and applications of inertial microfluidics: a review, *Lab on a Chip*, 2016, **16**, 10-34.

17. A. Karimi, S. Yazdi, and A. M. Ardekani, Hydrodynamic mechanisms of cell and particle trapping in microfluidics, *Biomicrofluidics*, 2013, **7**, 021501.

18. D. R. Gossett, W. M. Weaver, A. J. Mach, S. C. Hur, H. T. K. Tse, W. Lee, H. Amini, and D. Di Carlo, Label-free cell separation and sorting in microfluidic systems, *Analytical and Bioanalytical Chemistry*, 2010, **397**, 3249-3267.

19. M. Yamada, M. Nakashima, and M. Seki, Pinched flow fractionation: Continuous size separation of particles utilizing a laminar flow profile in a pinched microchannel, *Analytical Chemistry*, 2004, **76**, 5465-5471.

20. J. Takagi, M. Yamada, M. Yasuda, and M. Seki, Continuous particle separation in a microchannel having asymmetrically arranged multiple branches, *Lab on a Chip*, 2005, **5**, 778-784.

21. S. Choi and J.-K. Park, Continuous hydrophoretic separation and sizing of microparticles using slanted obstacles in a microchannel, *Lab on a Chip*, 2007, **7**, 890-897.

22. S. Choi, S. Song, C. Choi, and J.-K. Park, Continuous blood cell separation by hydrophoretic filtration, *Lab on a Chip*, 2007, **7**, 1532-1538.

23. R. D. Sochol, S. Li, L. P. Lee, and L. Lin, Continuous flow multi-stage microfluidic reactors via hydrodynamics microparticle railing, *Lab on a Chip*, 2012, **12**, 4168-4177.

24. R. D. Sochol, D. Corbett, S. Hesse, W. E. R. Krieger, K. T. Wolf, M. Kim, K. Iwai, S. Li, L. P. Lee, and L. Lin, Dual-mode hydrodynamic railing and arraying of microparticles for multi-stage signal detection in continuous flow biochemical microprocessors, *Lab on a Chip*, 2014, **14**, 1405-1409.

25. J. Lee and M. A. Burns, Asymmetric traps array for particle transport, *RSC Advances*, 2015, **5**, 3358-3364.

CHAPTER V

CONCLUSIONS AND FUTURE WORK

5.1 Conclusions

The overall aim of this dissertation work was to develop a new passive fluidic technique for spatial control of micro-particles in oscillatory flow. Our investigation of controlling of micro-particles lead us to utilize the physical interactions between the particle and physical obstacles, resulting in the design of the asymmetric trap that consists of three physical obstacles including a "barrier" and two "trapping blocks". The forced lateral displacement of the micro-particle by the barrier prevents the particle from trapping in forward flow, while those particles in reverse flow are captured by the trapping gaps. Capitalizing on this asymmetry of the physical interactions, we successfully developed the one-way particle transport, basic transport function of the asymmetric traps, in oscillatory flow. The theory we developed based on deterministic lateral displacement of micro-particles and mass balance relationships of fluid streams could explain the relationship between various regimes of particle dynamics and the critical dimension of the traps in oscillatory flow. Combining unique transport polarity of the asymmetric traps and particle dynamics predictable by our theory, we showed that the asymmetric traps could be used for segregation, medium exchange, and focusing and splitting of micro-particles.

Our first work started from designing a trap that can induce a change after a fluid oscillation, which results in the unique asymmetric interaction that traps a particle in reverse flow and avoids trapping in forward flow. We analyzed the effect of physical dimension including particle diameter and the gaps of the trap on the asymmetry of the interaction. In the process to quantify the critical dimension, we used a flow field obtained at the absence of a particle, which introduces an error. However, experimental validation showed the size of the error is negligible, and our method has the advantage of having a simpler calculation procedure for critical dimensions with acceptable accuracies.

Next, we tested the possibility of particle transport in the oscillatory flow. To achieve net positive displacement of particles in oscillatory flow, we defined four conditions: mechanical capturing, asymmetry, physical collision, and entering the capturing stream in reverse flow. Critical particle diameters for each condition were obtained separately, and they were merged into a single plot of the regimes of the trap-particle interactions at physical dimensions of the system. With the theory of lateral displacement of a particle in the periodic obstacle array, our model could predict particle dynamics in multiple rows of the asymmetric traps in oscillatory flow, which was experimentally confirmed based on the visual observation of trap-particle interaction. Among five regimes of trap-particle interactions, one-way particle transport could move the particles across tens of trap rows in a few fluid oscillations (the period of a oscillation < 500ms). The other interaction regimes showed no appreciable displacement of particles.

Lastly, based on the knowledge about the regimes of trap-particle interactions, we demonstrated practical functions including segregation, medium exchange, and focusing

and splitting of micro-particles. The segregation successfully isolated target particles of one-way particle transport regime from non-target particles of the symmetric capturing regime. The investigation of the effect of operation parameters on the segregation performances revealed that a number of particles at a given array capacity has a significant impact on the degree of segregation, yield, and purity of segregation product. The addition of an array of asymmetric traps enabled multiplexed segregation. Next, medium exchange of micro-particle was achieved by displacing the particles over mixing zone of two liquid mediums. We found that the medium exchange occurs at the modest amplitude and number of fluid oscillation. Lastly, we demonstrated focusing and splitting of micro-particles in multiple arrays of opposite direction.

5.2 Future Work

5.2.1 Cell Processing

Cell processing is a promising application area for the asymmetric traps. The asymmetric traps can conduct unit operations such as separation and medium exchange in a closed fluidic circuit, which makes this technique attractive for integrated Lab-on-a-Chip systems for cell processing without the need of any external intervention. The main difference between the micro-particles used for this work and cells is deformability. While Young's modulus (~1.9-2.9 GPa) of polystyrene micro-particles is high enough to ignore any deformation during the interaction with the trap, cells are much more deformable so that their hydrodynamic radius is decreased from their nominal diameter. This deformability difference will lead to the modification of the critical diameters we

obtained in the Chapter 2 and 3. Sorting of blood cells would be a good starting point of the test of cell processing.

5.2.2 Increasing Throughput with Deep Fluidic Channel

Increasing processing capacity with a microfluidic channel deeper than the current version of oscillatory flow device is a future work that will greatly improve the processing throughput of the asymmetric traps. Currently, the height of microfluidic channel used for the segregation is about 40 μm, which is barely double to the diameter of the non-target particle (d_p = 20.4 μm) and less than 1.5 times of the diameter of the target particle (d_p = 30.2 μm). Considering that the gap sizes of the asymmetric traps in the tested devices were the smallest dimensions that governed the particle dynamics, a deeper channel is expected to have the particle dynamics similar to it of the current shallow fluidic channel. The limit of maximum height is likely to be decided by the stability of the structure in the fabrication process. Prolonged dry etching causes undercut of the structure, and washing with liquids may break easily the structure of high aspect ratio.

5.2.3 Integration with a Microstructure for Manual Pumping of Fluid

The oscillatory flow of current devices relies on the expansion of the fluidic channel by flexible polymeric membrane actuated by vacuum. Integration of the array with a part for manual pumping for the oscillatory flow will enable a truly portable microfluidic device for micro-particle operations. For manual pumping of fluids, numerous techniques have been developed. The pumping lid is a good pumping element that can deliver defined volume of fluids at a pre-determined pressure. [1]

5.3 References

1. S. Begolo, D. V. Zhukov, D. A. Selck, L. Li, and R. F. Ismagilov, The pumping lid: investigating multi-material 3D printing for equipment-free, programmable generation of positive and negative pressures for microfluidic applications, *Lab on a Chip*, 2014, **14**, 4616-4628.

APPENDICES

APPENDIX A. The dimension of the asymmetric trap array for one-way particle transport

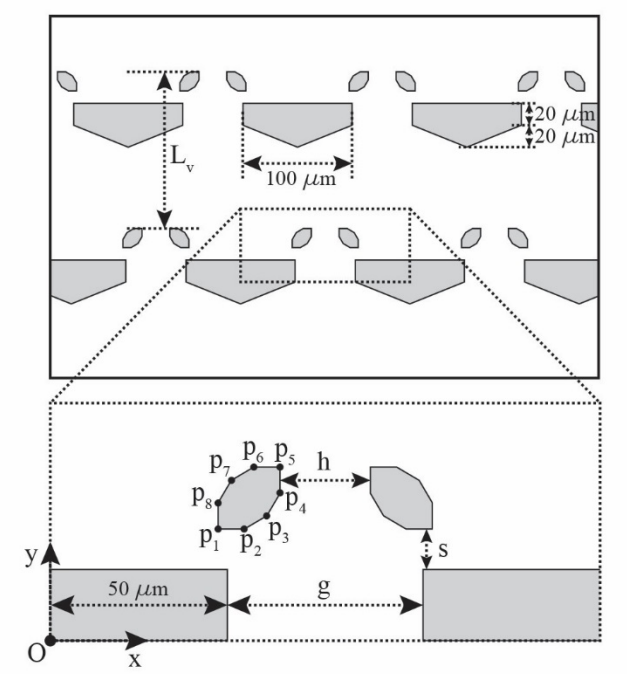

Figure A.1: Dimension of the asymmetric trap array

Variables	Coordinate [x , y]
L_v (length in μm)	2*[Round up (s + p_1(y) – p_5(y) + 40) by 5]
p_1	[50-(g-h)/2*tan(15^o) , s]
p_2	[54-(g-h)/2*tan(15^o) , s]
p_3	[50+(g-h)/2*(1-tan(15^o)) , s+(g-h)/2*tan(15^o)]
p_4	[50+(g-h)/2 , s+(g-h)/2*(1+tan(15^o))-4]
p_5	[50+(g-h)/2 , s+(g-h)/2*(1+tan(15^o))]
p_6	[46+(g-h)/2 , s+(g-h)/2*(1+tan(15^o))]
p_7	[50 , s+(g-h)/2]
p_8	[50-(g-h)/2*tan(15^o) , s+4]

Table A.1: Length and coordinates of the variables.

Appendix B. Geometry for Finite Element Method (FEM) simulation

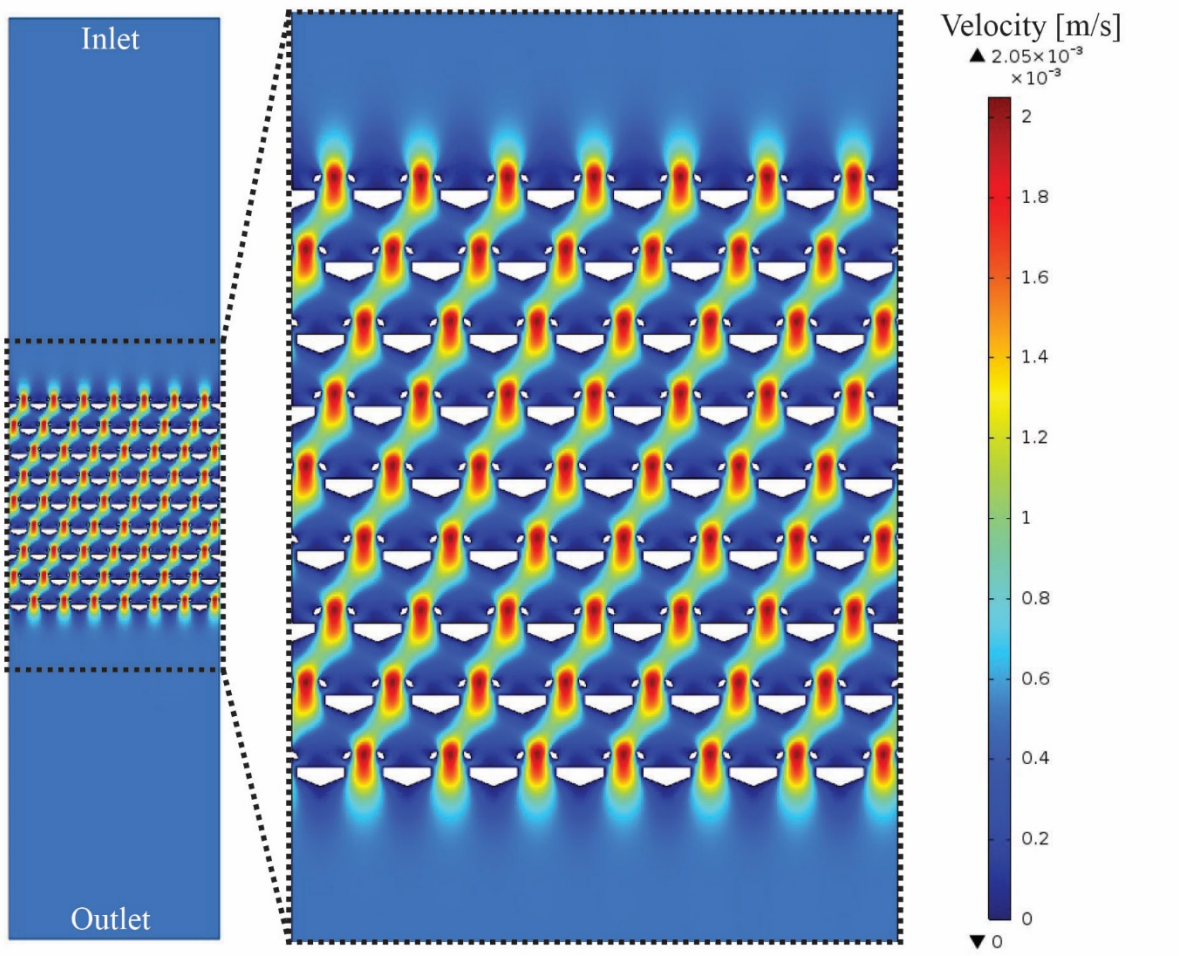

Figure B.1: Velocity plot of the FEM simulation results. Flat inlet and outlet ensures average vertical velocity across the asymmetric trap array. Flow rate of each gap was calculated by averaging flow rates obtained at five different locations in central region of the array. The array dimension shown here is $\varepsilon = 1/3$, $g^* = 1.5$, and $s^* = 0.3$.

Appendix C. The modified equation for b_r and b_l in the case that $Q_s \leq Q_{unit} \leq 2Q_s$

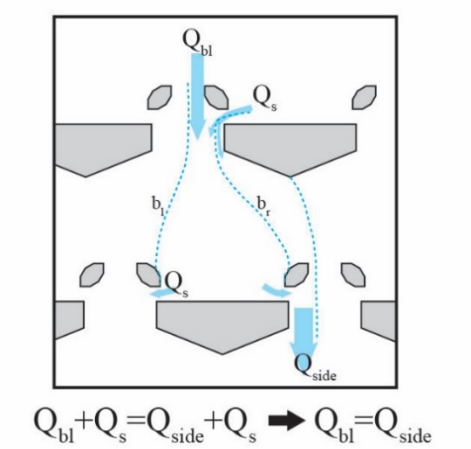

Figure C.1: Modified mass balance relationship when $Q_s \leq Q_{unit} \leq 2Q_s$ at larger trapping gap size. Since the rightmost boundary streamline, b_r, of the capturing stream is outside the inter-trapping blocks gap (h), Q_{br} is equal to zero.

Appendix D. The lateral shift into the capturing stream at different trapping gap sizes (0.1-0.5)

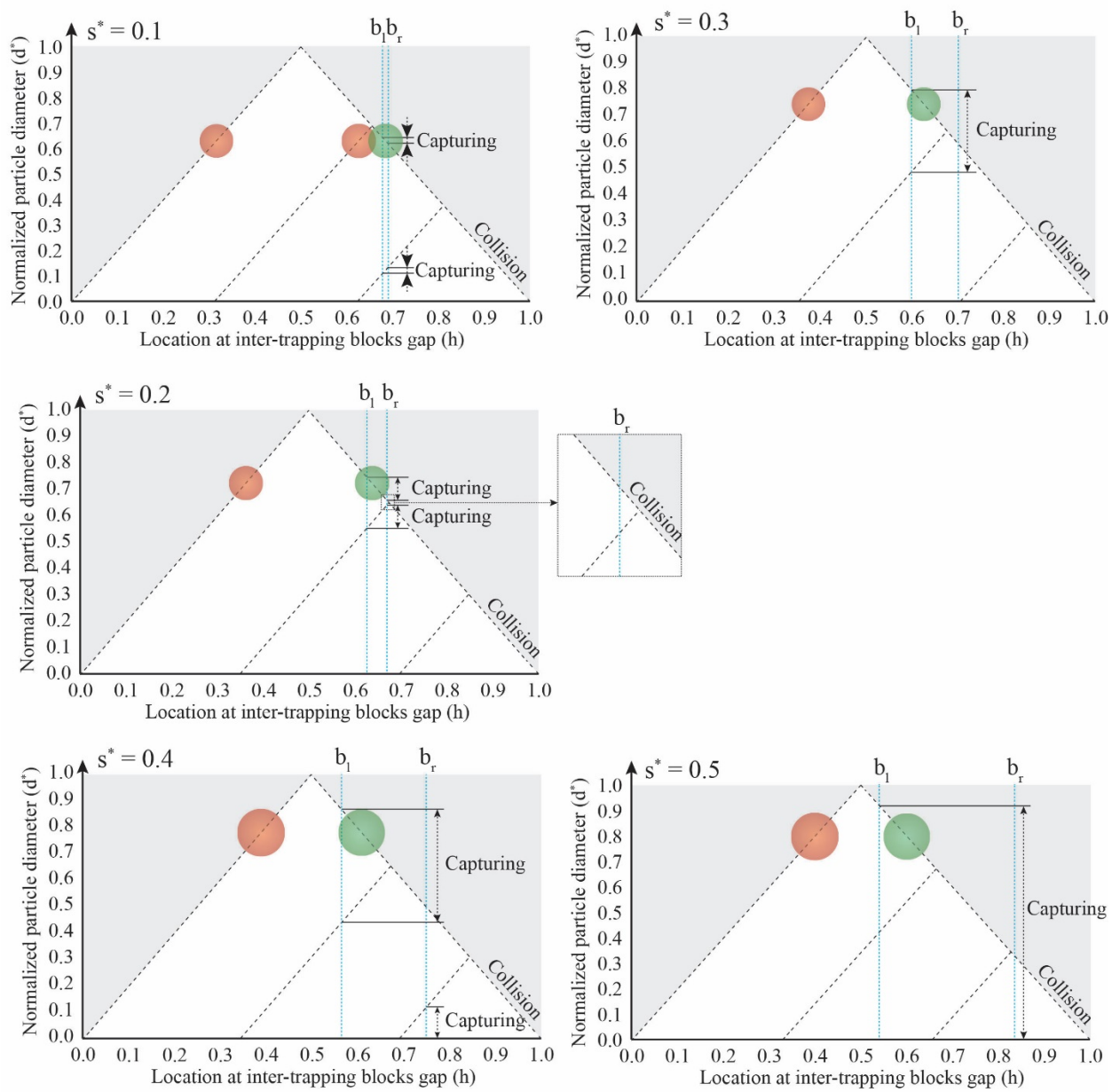

Figure D.1: The lateral shift of the particle into the capturing stream at different trapping gap sizes ($0.1 \leq s^* \leq 0.5$)

Appendix E. Phase diagrams at various row shift fractions (ε = 1/5, 1/4, 1/3, and 1/2)

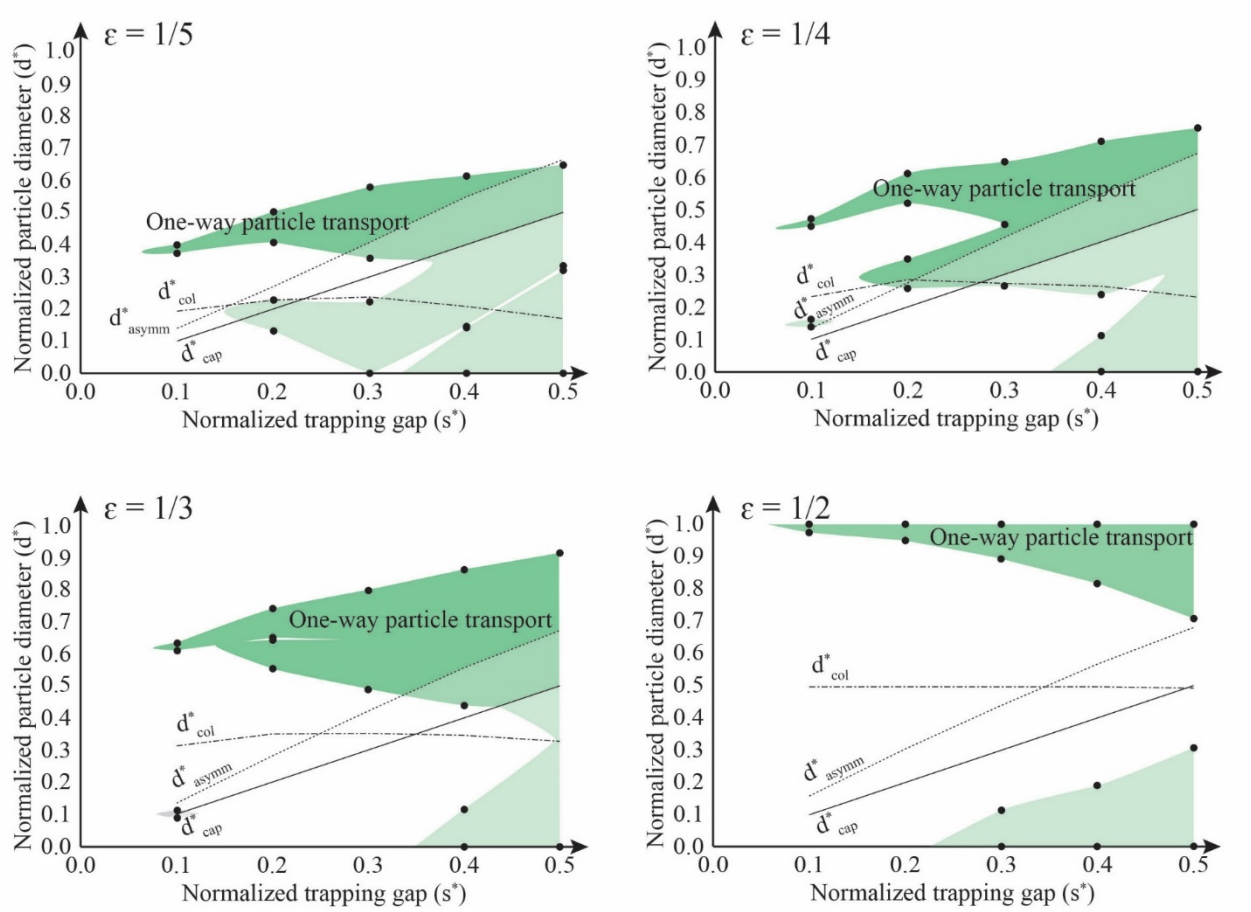

Figure E.1 Phase diagrams at different row shift fractions (ε = 1/5, 1/4, 1/3, and 1/2). The black dots in the graphs are the intersections between the location of the capturing stream and lateral location of the particle center in reverse flow at five normalized trapping gap sizes (s* = 0.1, 0.2, 0.3, 0.4, and 0.5). It should be noted that the line between the calculated points were interpolated based on the trend of diameter range at two trapping gap sizes.

Appendix F. Alternating the sign of row shift angle

Taking account of experimental implementation of the one-way particle transport, the sign of the row shift angle should be alternated to prevent undesired particle concentration at the region near channel sidewall (Figure S.6). Large particles show bump mode transport[41], a type of particle transport following the direction of row shift by capitalizing on the particle collision at every row of the trap array. The bump mode transport cause the area near the side wall of the array that has only a single sign of row shift angle becomes crowded with particles as distance of forward transport increases. This unwanted particle concentration increases the probability of channel clogging and may cause errors in the operation of the one-way particle transport. Alternating the sign of the row shift angle can minimize the particle crowding by guiding the particles to opposite direction before they reach to the sidewall area.

To keep the conditions for the one-way particle transport unchanged, a sign of the row shift angle have to be kept for at least 1/ε rows of the traps. Although this design doubles the flow periodicity of the array from 1/ε rows to 2/ε rows, the conditions about the physical collision and the lateral shift into the capturing stream are viable in 1/ε rows so that the amplitude of 2/ε rows achieve one-way particle transport. By placing one row of traps at the inlet of the array at first and adding 1/ε rows of the traps with alternated sign of the row shift angle, an array with the sign of the row shift angle fixed for 1/ε trap rows can be designed.

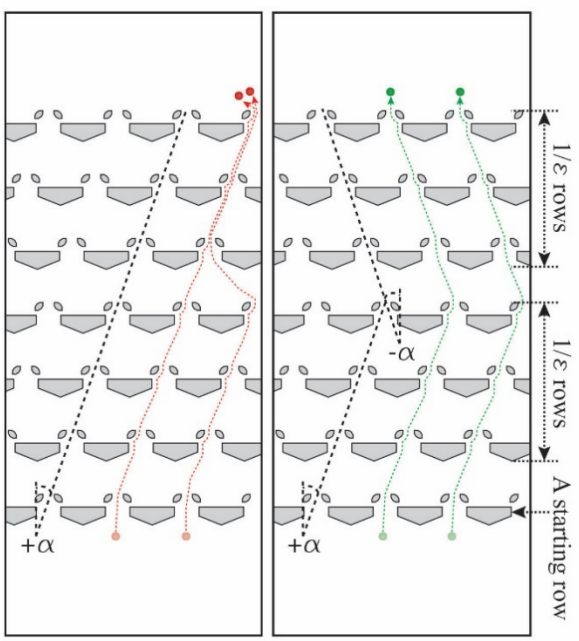

Figure F.1: Undesired local particle concentration (left) in the area near channel sidewall can be avoided by alternating the sign of the row shift angle from +α to –α, or vice versa (right). The array was designed to have a fixed sign of the row shift angle for 1/ε rows of the traps. This design allows the results of the d^*_{col} and the lateral shift into the capturing stream to remain valid while alternating sign of the row shift angle.

Appendix G. Bandwidth of target (one-way particle transport) and non-target (symmetric capturing) particles

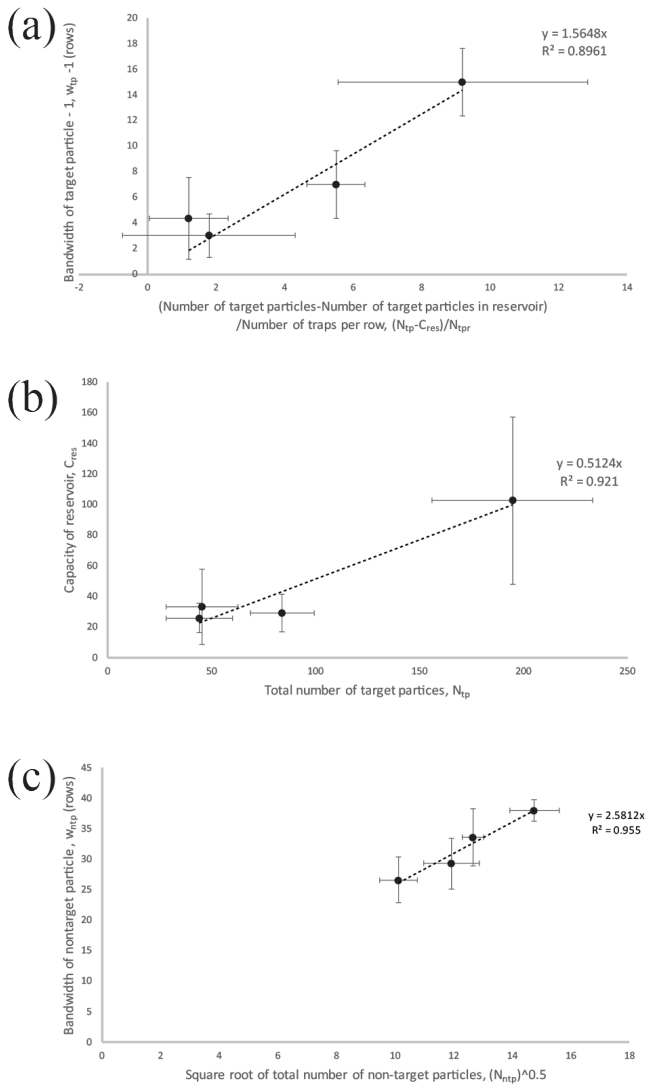

Figure G.1: Bandwidth of target (one-way particle transport) and non-target (symmetric capturing) particles. (a) The bandwidth of target particles as function of the number of target particles in the array. (b) The capacity of the reservoir as a function of total number of target particles. (c) The bandwidth of non-target particles as a function of square root of total number of non-target particles